Cerebellum (2012) 11:85–101
DOI 10.1007/s12311-010-0216-3

Models of Calcium Dynamics in Cerebellar Granule Cells

Elena È. Saftenku

Published online: 5 October 2010

Abstract Intracellular calcium dynamics is critical for many functions of cerebellar granule cells (GrCs) including membrane excitability, synaptic plasticity, apoptosis, and regulation of gene transcription. Recent measurements of calcium responses in GrCs to depolarization and synaptic stimulation reveal spatial compartmentalization and heterogeneity within dendrites of these cells. However, the main determinants of local calcium dynamics in GrCs are still poorly understood. One reason is that there have been few published studies of calcium dynamics in intact GrCs in their native environment. In the absence of complete information, biophysically realistic models are useful for testing whether specific Ca^{2+} handling mechanisms may account for existing experimental observations. Simulation results can be used to identify critical measurements that would discriminate between different models. In this review, we briefly describe experimental studies and phenomenological models of Ca^{2+} signaling in GrC, and then discuss a particular biophysical model, with a special emphasis on an approach for obtaining information regarding the distribution of Ca^{2+} handling systems under conditions of incomplete experimental data. Use of this approach suggests that Ca^{2+} channels and fixed endogenous Ca^{2+} buffers are highly heterogeneously distributed in GrCs. Research avenues for investigating calcium dynamics in GrCs by a combination of experimental and modeling studies are proposed.

Keywords Calcium dynamics · Mathematical model · Calretinin · Endogenous buffers

E. È. Saftenku (✉)
Department of General Physiology of Nervous System,
A. A. Bogomoletz Institute of Physiology,
4 Bogomoletz St.,
Kyiv 01024, Ukraine
e-mail: esaft@biph.kiev.ua

Introduction

In recent years, significant progress has been made in the extent, speed, and resolution of imaging in vitro and in vivo. The development of laser scanning microscopy [1, 2] and optimization of synthetic and protein-based indicators [3] now allows fast multi-site functional imaging of neurons across the different spatial scales [4] and examination of calcium signals within highly localized microdomains [5] and small cellular compartments such as dendrites and spines [6]. At the same time, the interpretation of Ca^{2+} imaging data has become more complex. Although it is evident that selective triggering of neuronal functions is often achieved through spatial localization of calcium signals within an extremely confined space or in a larger sub-region of the cell [6–8], the precise mechanisms determining the spatial domains are not always clear. Exploration of the individual contribution of Ca^{2+} handling systems is complicated because of their functional interdependence and the lack of experimental data that specify the properties and distribution of all Ca^{2+} transport systems in the same cell type. Effective methods for measurement and analysis of Ca^{2+} fluxes in intact cells have been recently developed, but hitherto they were applied only to sympathetic neurons [9]. One approach to overcoming these difficulties is mathematical modeling, which is an indispensable tool for determining the spatio-temporal properties of Ca^{2+} signals expected for a given collection of Ca^{2+} handling systems operating in a cell with defined geometry. This approach can be used both to determine if a particular collection of Ca^{2+} handling systems is adequate to account for a set of experimental observations and to suggest experiments that help distinguish between competing models.

For cerebellar granule cells (GrCs), which constitute about 70% of all neurons in the rat [10] and 80% in the

human [11–13] brain, surprisingly little is known about Ca^{2+} dynamics compared to other types of neurons. This situation needs to be changed not only because Ca^{2+} regulates almost all forms of neuronal activity, e.g., gene expression [14, 15], transmitter release [16], short-term and long-term synaptic plasticity [17, 18], membrane excitability [19], and different forms of cell death [20–22] studied in GrCs, but also because GrCs seem to have special mechanisms of Ca^{2+} handling. Being the smallest neurons in the brain, with a diameter of only 5–10 μm in different species [23], and supporting Ca^{2+} influx and sustained vesicular release at high rates at each release site of mossy fiber (MF) to GrC synapses [24], GrCs can fire in vivo up to 250 Hz continuously without accommodating [25, 26]. Therefore, elucidation of specializations that enable GrCs to maintain Ca^{2+} homeostasis is of special interest. Here, we describe the key Ca^{2+} regulatory mechanisms in GrCs and show how the analysis of computational models sheds new light on experimental observations.

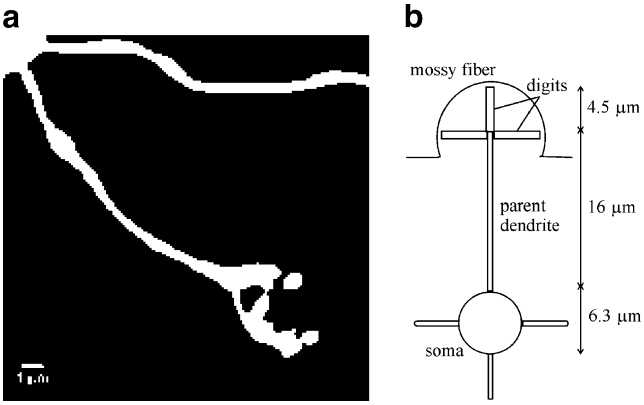

Fig. 1 Morphological structure of cerebellar GrC. **a** Confocal image of a mature GrC filled with biocytin. A dendritic terminal with claw-like digits is shown. Reprinted from [18] with permission from the Journal of Neuroscience. **b** Schematic representation of a GrC morphology used in the model study [140]. The model cell consisted of a soma and four dendrites, each of which ended with three digits. The dendrites had a diameter of 0.5 μm, and the digits had a diameter of 0.76 μm

Experimental Study of Calcium Signaling in GrCs

Components of Ca^{2+} Regulation

Synaptic Receptors

Evoked increases in cytosolic Ca^{2+} arise in GrCs from three general sources: NMDA receptors (NMDARs), voltage-sensitive Ca^{2+} channels, and release from internal stores. A mature GrC has only four short dendrites (range, 3–5), which receive a single excitatory MF input each and terminate with, on average, three digits where glutamatergic synapses are situated [18, 27–29] (Fig. 1). The majority of the AMPA receptors in the synapses of cerebellar GrCs are heteromeric channel assemblies containing GluR2 subunits [30]. The GluR2 mRNA is completely edited at its Q/R site almost at birth [31, 32]; therefore, AMPA receptors are Ca^{2+}-impermeable [33]. The extent of RNA editing of kainate-type channels increases as GrCs maturate [34]. However, high-affinity kainate receptors are not involved in synaptic transmission even in neurons of young animals [30, 35]. The majority of NMDARs in mature GrCs are located outside the synaptic specializations and are activated by glutamate spillover [29]. The fraction of the total NMDAR-mediated current that is carried by Ca^{2+} is about 10% [36].

Ca^{2+} Channels

Four types of Ca^{2+} channels were distinguished pharmacologically in cultured rat GrCs, P/Q- (46%), N- (20%), R- (19%), and L-type (15%) [37], whereas currents measured in slices of mature cerebellar GrCs were mostly of N-type and did not contain components sensitive to the P/Q channel antagonist [38]. In presynaptic boutons of immature GrCs, P/Q- (48%), N- (27%), and R-type (23%) calcium channels were identified [16, 39]. In adult rats, immunostaining for the α_{1A} subunit of P/Q-type channels was observed only in the parallel fiber varicosities [40]. However, in leaner mutant mice, which carry autosomal recessive mutations in the gene coding for this subunit and show severe ataxia and epilepsy, cerebellar GrCs have significantly lower basal levels of cytosolic free calcium concentration ($[Ca^{2+}]_i$) in comparison with wild-type mice [41]. This suggests, perhaps, a necessity of Ca^{2+} entry through P/Q-type channels for a normal homeostasis at an earlier stage of development.

Plasma Membrane Exchangers and Pumps

Calcium is extruded from GrCs by K^+-independent (NCX) and K^+-dependent (NCKX) Na^+/Ca^{2+} exchangers [42, 43] and Ca-ATPases (PMCA; four isoforms [44, 45]). Prominent labeling of PMCA was observed in the digits and soma [46]. However, a rapidly activating PMCA2a isoform was observed only in the glomeruli [47]. Recently, it was shown that $[Ca^{2+}]_i$ clearance in the soma of cultured GrCs stimulated by pulses of 60 mM KCl (≤10 s) relies almost completely on the PMCA [48]. The distribution and contribution of different NCX and NCKX isoforms to Ca^{2+} removal from the cytosol and neuronal functions of GrCs have not yet been investigated, although several studies have demonstrated a prominent role for NCKX in calcium extrusion from axon terminals of other neurons [49].

Endoplasmic Reticulum

For a long time, GrCs have been known to contain mitochondria [23, 50, 51] and endoplasmic reticulum (ER) [23, 52] in the soma and digits, but physiological role of these organelles in Ca^{2+} handling of GrCs under normal physiological conditions is still not well understood. Ca^{2+}-induced Ca^{2+} release (CICR) and IP_3-induced Ca^{2+} release (IICR) from the ER were observed both in GrC cultures (e.g., [53, 54]) and in slices [18, 55]. Physiological activation of IICR requires stimulation of plasmalemmal receptors coupled with phospholipase C, which cleaves phosphatidylinositol-4,5-biphosphate (PIP_2) into diacylglycerol and inositol-1,4,5-trisphosphate (IP_3), and the latter induces Ca^{2+} release from the ER [56, 57]. In GrCs, phospholipase C was shown to be activated by muscarinic, histaminergic, α-adrenergic, and metabotropic glutamate receptors (mGluRs; mGluR1a isoform) [58–63]. mGluRs are preferentially localized at the periphery of postsynaptic densities [64] and are stimulated by synaptic activities. Ca^{2+} in GrCs is also released from the ER via ryanodine receptor channels (RyRs, cardiac type [65]) and leak pathways [66]. It has not been shown whether Ca^{2+} entry through synaptically stimulated NMDARs activates CICR in slices. There is some evidence that mGluRs can also activate RyRs independently of IP_3-mediated Ca^{2+} mobilization, but these effects were observed only in developing cultured GrCs [67]. Ca^{2+} uptake into the ER is mediated by sarcoplasmic/ER Ca^{2+}-ATPases (SERCAs; 2b isoform [44]). In the ER, Ca^{2+} is stored bound to proteins; the major Ca^{2+}-binding protein in neurons is calreticulin [68].

Ca^{2+} release from the ER of GrCs may follow by Ca^{2+} influx through store-operated calcium (SOC) channels [69] (but see also [70]). SOC entry amplitude is typically very low compared to $[Ca^{2+}]_i$ signals mediated by voltage-dependent Ca^{2+} channels upon depolarization [71]. However, it may influence the decay of synaptically [72] and, probably, depolarization-induced Ca^{2+} transients. The influx through SOC channels is activated by targeted migration of stromal interacting molecule 1 (STIM1) and STIM2 proteins to ER cisternae puncta located underneath the plasma membrane (PM) [73, 74]. STIM2 is considered to be the primary regulator for basal Ca^{2+} influx, while both STIM1 and STIM2 trigger Ca^{2+} influx following ER store depletion [74]. Moderate STIM1 immunoreactivity was observed in the granular layer of the cerebellum [75], but further investigations are necessary to examine whether STIM1 and STIM2 channels are indeed present in GrCs.

Mitochondria

Mitochondria influence Ca^{2+} signals by acting as sophisticated high-capacity buffers and by clearing Ca^{2+} in restricted microdomains [76]. They accumulate Ca^{2+} via the electrogenic Ca^{2+} uniporter in the inner mitochondrial membrane and release Ca^{2+} to the cytosol through the Na^+/Ca^{2+} exchanger [77, 78]. In GrCs, the role of mitochondria was examined mainly in cellular pathology associated with glutamate excitotoxicity [20, 79–83]. It was shown that during brain injury or during hypoxic/ischemic insults, glutamate accumulation leads to overactivation of extrasynaptic NMDARs, inappropriate levels of Ca^{2+} influx, and neuronal cell death [84]. Current theories suggest that mitochondrial calcium uptake plays a central role in this process [20, 80, 82, 83, 85]. Severe hypoxia/ischemia may lead to a delayed Ca^{2+} deregulation [81], rapid and complete loss of mytochondrial membrane potential, ATP depletion, mitochondrial damage, and acute necrotic cell death [20, 79, 83]. Neurons experiencing less severe hypoxic/ischemic episodes may suffer only a transient or incomplete mitochondrial depolarization due to increased Ca^{2+} uptake [21, 79, 83]. Excessive uptake of Ca^{2+} by mitochondria causes the release of cytochrome c and other proapoptotic factors that initiate the executor caspase cascade [86]. Chronic neurodegenerative diseases are also associated with dysregulation of Ca^{2+} homeostasis and mitochondrial dysfunction [76, 87]. In contrast, physiological synaptic NMDAR activity has neuroprotective effect [88, 89].

Cytosolic Endogenous Buffers

Several Ca^{2+}-binding endogenous buffers were identified in cerebellar GrCs [90]. It is likely that calretinin is the main buffer that is expressed in these cells [19, 90]. The intensity of the calretinin immunostaining in GrCs varies significantly in different cerebellar regions [91–93]. Recently, the kinetics of Ca^{2+} binding to calretinin was assessed by using UV flash photolysis of DM-nitrophen in combination with model-based analysis of fluorescence transients. This study revealed that calretinin has two pairs of cooperative Ca^{2+}-binding sites with an initial slower and a second faster Ca^{2+} binding step and one independent site with a relatively slow rate of Ca^{2+} binding [94]. Calretinin-deficient mice present motor discoordination [95] because of changes in intrinsic excitability of GrCs that influence computation in the cerebellar cortex [96]. Several other proteins found to be expressed in rat GrCs, calmodulin [97], the neuronal visinin-like proteins NVP1 and NVP3, and frequenin (NCS-1) [98], also have cooperative binding kinetics with Ca^{2+} and can be associated with the PM [99]. The up-to-date knowledge about Ca^{2+} pathways in mature GrCs is schematically presented in Fig. 2.

Evidence of Spatially Segregated Ca^{2+} Signals in Grcs

In the past two decades, $[Ca^{2+}]_i$ was recorded mainly in groups of GrCs [54, 100, 101], in the populations of GrC

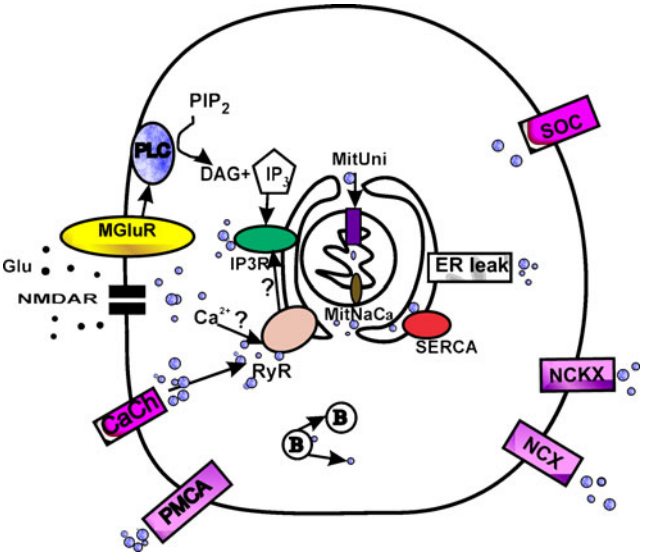

Fig. 2 Calcium handling in a mature cerebellar GrC. *Question marks* label the signaling pathways that have not been shown in experiments carried out in slices. *CaCh* voltage-gated Ca^{2+} channels, *NMDAR* NMDA receptors, *Glu* glutamate, *MGluR* metabotropic glutamate receptors, *PMCA* plasma membrane (PM) Ca^{2+} ATPase, *NCX* PM sodium–calcium exchangers, *NCKX* PM potassium-dependent sodium–calcium exchangers, *PLC* phospholipase C, PIP_2 phosphatidylinositol-4,5-bisphosphate, IP_3 inositol-1,4,5-trisphosphate, *DAG* diacylglycerol, IP_3R IP_3 receptors, *RyR* ryanodine receptors, *SERCA* sarco/endoplasmic reticulum Ca^{2+}-transporting ATPases, *ER leak* leak pathways from the endoplasmic reticulum, *MitUni* mitochondrial electrogenic Ca^{2+} uniporters, *MitNaCa* mitochondrial Na^{+}–Ca^{2+} exchangers, *SOC* store-operated channels, *B* endogenous buffers

presynaptic terminals [16, 39, 102–106], and in the soma of single GrCs [48, 53, 55, 59, 80, 107–115]. Only recently, a few studies have begun to examine calcium dynamics in the individual presynaptic boutons [116–118] and GrC dendrites [18, 119]. These studies revealed large differences in $[Ca^{2+}]_i$ responses among presynaptic boutons and segregated Ca^{2+} signaling in dendrites. Ca^{2+} transients of different amplitude and duration were measured in the neurites and soma of cultured GrCs during perfusion with a high potassium solution or NMDA application [119]. In the most detailed study of calcium dynamics in mature GrCs in slices, Gall et al. [18] showed that the peak amplitudes of fluorescence transients induced by either synaptic stimulation or depolarizing voltage steps decreased progressively and significantly with distance from the dendritic endings (Fig. 3). Furthermore, the peak amplitude of $[Ca^{2+}]_i$ elevations in the dendritic endings attained during presynaptic stimulation determined the occurrence and the sign of long-term synaptic plasticity, depression or potentiation, at MF−GrC synapses. Depolarization-induced Ca^{2+} entry in the digits of GrCs was significantly protracted and amplified by CICR, whereas synaptically evoked Ca^{2+} transients were almost abolished in the presence of NMDAR blockers and decreased to a lesser extent in the presence of mGluR1 antagonist [18] (Fig. 4). No attempts have been made to clarify the underlying mechanisms responsible for generating spatially heterogeneous Ca^{2+} transients in different cell compartments.

Difficulties in Experimental Study of Ca^{2+} Handling

There are several difficulties in experimental study of Ca^{2+} handling in cerebellar GrCs. (1) Pharmacological activation of signaling pathways in GrCs that involve Ca^{2+} entry and different aspects of excitotoxicity were explored mainly in cultured neurons [48, 53, 54, 59, 80, 82, 101, 107–115, 119], which are usually maintained under chronic depolarizing conditions (at 20–30 mM potassium). Survival-promoting depolarization changes expression of different channels, receptors and transporters and prevents the maturation process of GrCs [44, 55, 120–127]; therefore, Ca^{2+} handling mechanisms also may be altered. But only in few cases were the measurements of $[Ca^{2+}]_i$ performed in GrCs studied in cerebellar slices [18, 55, 69, 116–118]. (2) Measuring $[Ca^{2+}]_i$ requires the introduction of fluorescent indicators that necessarily disrupt normal Ca^{2+} signaling [6]. If dye-loading via a patch pipette is used and mobile endogenous buffers are washed out during whole-cell recordings, synthetic calcium buffers cannot replicate cellular buffering in the presence of mobile endogenous buffers with cooperative Ca^{2+}-binding kinetics, especially under different experimental conditions. Therefore, the prediction of calcium dynamics in unperturbed GrCs is required. (3) Even if the distributions of all the receptors, channels, buffers, pumps, and exchangers are determined, the computational simulations are necessary to achieve an understanding on how nonlinear interactions between all Ca^{2+} handling systems produce very specific Ca^{2+} responses. On the other hand, a complete biophysical model of Ca^{2+} signaling in cerebellar GrCs is possible only after experimental study and description of all components of Ca^{2+} regulation immediately in these cells. Therefore, to understand calcium dynamics in GrCs, many more experiments must be carried out in cerebellar slices and combined with modeling approaches.

Phenomenological Models of Calcium Dynamics in GrCs

A number of one-compartmental models of neuronal activity in GrCs [19, 128–132] include a phenomenological description of calcium dynamics:

$$\frac{d[Ca^{2+}]_i}{dt} = f\left(\frac{I_{Ca}}{2FV_d} - \beta\left([Ca^{2+}]_i - [Ca^{2+}]_{rest}\right)\right). \quad (1)$$

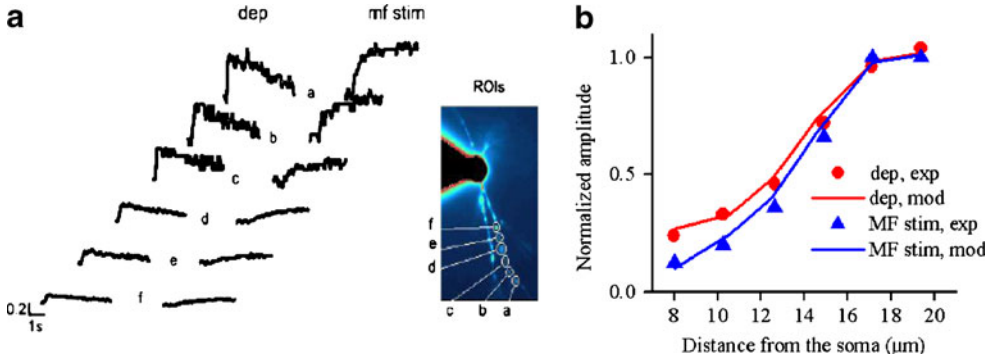

Fig. 3 Spatial profiles of experimental fluorescence and simulated concentration changes of bound with Ca^{2+} indicator Oregon Green BAPTA-1 ([CaOGB1]). **a** Ca^{2+} transients are measured at different dendritic positions (**a**–**f**) and are induced either by a 200-ms depolarization from −70 to 0 mV or by high-frequency MF stimulation (1 s at 100 Hz) while holding the cell at −70 mV in the absence of extracellular Mg^{2+}. The fluorescence change decreases from the dendritic ending to the middle of the parent dendrite. The *inset* shows a fluorescence image with indication of the regions of interest *a*–*f* used for fluorescence measurements. Reprinted from [18] with permission from the Journal of Neuroscience. **b** Comparison of normalized amplitudes of measured fluorescence transients elicited by depolarization and synaptic stimulation as in **a** (*symbols*) and normalized amplitudes of simulated changes in [CaOGB1] (*lines*) at different distances from the soma. For simulations of depolarization-induced fluorescence transients, Ca^{2+} conductance in the parent dendrites was set ~4 times lower than in the digits and Ca^{2+}-induced Ca^{2+} release was included only in the digits of the model cell. The best fit of the spatial profile of synaptically induced fluorescence transients was obtained using the model with the diffusion coefficient of OGB1 (D_{OGB1}) 15 $\mu m^2 s^{-1}$ and inositol-1,4,5-trisphosphate-induced Ca^{2+} release included only in the digits of GrCs. The maximum fluorescence change $(\Delta F/F)_{max}$ for these simulations was set at 0.6. Simulations with different $(\Delta F/F)_{max}$ (0.4–0.6) and concentration of uniformly distributed buffer (0–600 μM) did not influence significantly the goodness of fit and D_{OGB1} estimates. Adapted from [140] with permission from Elsevier Science

Here, f is the buffer capacity of intracellular buffers, I_{Ca} is the calcium current, V_d is the volume of the submembrane shell, F is the Faraday constant, β is the rate constant of $[Ca^{2+}]_i$ decay. In the multicompartmental GrC model of Gabbiani et al. [133], calcium dynamics was taken into account only in the soma. In another study [134], the I_{Ca} and the Ca^{2+}-activated K^+ current (I_{KCa}) were placed only in the apical part of the dendrites. Phenomenological models were useful for simulation of I_{KCa}, but they did not reproduce realistic $[Ca^{2+}]_i$ changes in GrCs. The amplitudes of Ca^{2+} transients during repetitive action potentials (APs) ranged in different models from 200 nM [131] to 14 μM [134]. The distribution of Ca^{2+} and Ca^{2+}-activated K^+ channels in real GrCs also may be different. Indeed, a comparable density of I_{Ca} in the soma and in the digits may result in much lower Ca^{2+} transients in the former compartment [18] because of the difference in the surface-to-volume ratio.

Even with such simple models, some general suggestions about a role of calcium dynamics in GrCs can be obtained. Gall et al. [19] nicely demonstrated that an increase in GrC excitability observed in calretinin-deficient mice may be explained by a decreased cytosolic Ca^{2+} buffer capacity if Ca^{2+} accelerates activation of I_{KCa} without changing its amplitude. To prove this possibility, the realistic kinetic description of large-conductance Ca^{2+}-activated K^+ (BK_{Ca}) channels [135], which are expressed in cerebellar GrCs [136], would need to be obtained experimentally and included in the model. Using the same model as in [19], Roussel et al. [131] suggested that the V_d in Eq. 1 corresponds to the total volume of the digits and that Ca^{2+}-activated K^+ channels in GrCs are regulated by nanomolar Ca^{2+} changes. However, application of the blocker of Ca^{2+}-activated small conductance K^+ channels did not affect any excitable responses in GrCs [137], whereas robust activation of cloned BK_{Ca} channels requires values for $[Ca^{2+}]_i$ of ≥10 μM at physiological potentials [138, 139]. Therefore, Ca^{2+}-activated K^+ channels in GrCs are not likely to be operated by low regional $[Ca^{2+}]_i$ changes, but rather by Ca^{2+}-nano/microdomains that form in the immediate vicinity of active Ca^{2+} sources. A study of functional coupling between different types of Ca^{2+} channels and BK_{Ca} channels in cell-attached patches of GrCs is an actual, but challenging task that needs to be performed for understanding the regulation of neuronal firing patterns in these cells.

A Biophysical Model of Calcium Dynamics in GrCs: Problems and Approaches

Recently, we proposed a biophysical model of calcium dynamics in GrCs [140]. The rates of $[Ca^{2+}]_i$ change in each intracellular compartment, the cytosol, ER, and mitochondria, were described by a set of differential equations. These rates depended on Ca^{2+} diffusion, buffering and the Ca^{2+} fluxes across the PM and/or membranes of intracellular compartments. The model was used to simulate

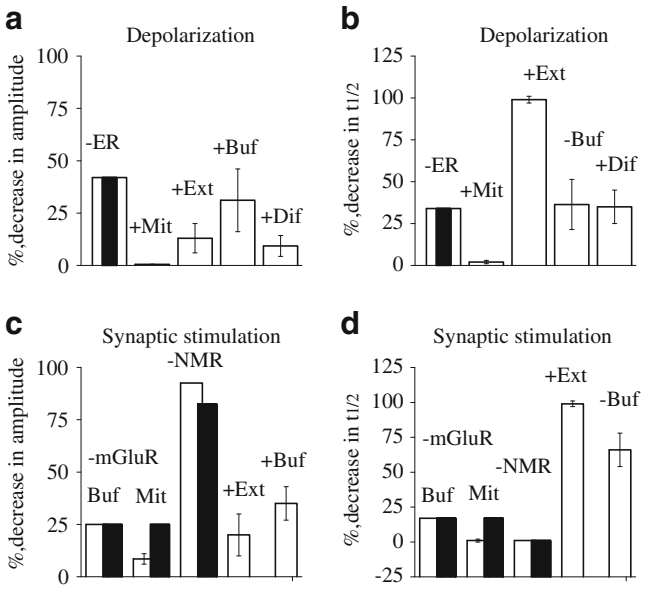

Fig. 4 Effects of the elimination and addition of different components of Ca^{2+} transport on Ca^{2+} responses evoked by depolarization and synaptic stimulation. The values of the percentage decrease in the amplitude (**a**, **c**) and half-decay time ($t_{1/2}$) (**b**, **d**) of simulated [CaOGB1] transients in the digits of GrCs are shown. Simulations were performed to reproduce the measured characteristics of fluorescence transients (*filled columns*) after preincubation of GrCs with thapsigargin that resulted in elimination of ER Ca^{2+} transport (−ER) or after application of NMDA receptor (−NMR) and metabotropic glutamate receptor (−mGluR) blockers. The latter effect was simulated in the model with a high-affinity buffer (Buf) placed to the apical part of the digits and in the model with mitochondria (Mit) in the GrC digits. The effects of the addition to the model of mitochondrial transport (+Mit), extrusion mechanisms (+Ext), axial diffusion (+Dif), and the addition (+Buf) or elimination (−Buf) of endogenous buffers are shown. The graphs combine the results of simulations reproducing fluorescent transients under different experimental conditions. The addition of extrusion mechanisms resulted in an increase of the amplitude of simulated transients only by several percents if endoplasmic reticulum Ca^{2+} transport was abolished

$[Ca^{2+}]_i$ responses recorded in the experiments of Gall et al. [18]. Our simulations benefited from the choice of experimental protocol in [18] that allowed separate examination of Ca^{2+} transients induced by activation of synaptic receptors and Ca^{2+} entry through voltage-dependent Ca^{2+} channels. Mathematical descriptions of depolarization-induced calcium [130] and NMDAR-mediated currents [132], which were measured in GrCs of the same age [38, 132] as in [18], were already obtained previously. However, we faced problems with simulations of Ca^{2+} responses in GrCs. First, in spite of a number of biophysically realistic models of calcium dynamics were developed for other cells (e.g., [141–148]) and the modes to describe Ca^{2+} regulatory systems are known, a general problem of most of these models is a lack of the data derived from experiments with the same cells. Second, the experiments regarding the contribution of different handling systems in Ca^{2+} signaling in cerebellar GrCs are still incomplete. Thus, in the only work where $[Ca^{2+}]_i$ was measured in the dendrites and soma of GrCs in slices [18], the inhibitors of mitochondrial uptake were not used, the relative contribution of different Ca^{2+} extrusion mechanisms across the PM was not estimated, and even the maximal fluorescence change ($(\Delta F/F)_{max}$) necessary to translate fluorescence into $[Ca^{2+}]_i$ was not determined. Third, although the main components of Ca^{2+} regulation in GrCs are known, the spatial and temporal interplay of these components is much less understood.

Therefore, we have devised an approach that can be applied for study of the distribution of Ca^{2+} handling systems in the conditions of insufficient experimental data. Its main features are: (1) investigating the cases of increasing complexity, comparing the measured and simulated $[Ca^{2+}]_i$ responses; (2) testing various hypotheses about the distribution and properties of Ca^{2+} handling systems (calcium channels, extrusion mechanisms, endogenous buffers, ER, and mitochondria) in the context of a realistic description of cell morphology and model parameters and rejecting those hypotheses that do not match experiments; (3) simulations within all the space of allowable ranges of uncertain parameters and their combinations; (4) in the case of the absence of experimental data, the use of the least favorable for a particular hypothesis parameters. This strategy helps to elaborate the most likely hypotheses that can be then tested experimentally.

In our model [140], the uncertain parameters mentioned in the item (3) above were: the resting calcium concentration, the total concentration of a uniformly distributed fixed buffer, the $(\Delta F/F)_{max}$, and the diffusion coefficient of the Ca^{2+} indicator Oregon Green BAPTA-1 (OGB1). The latter parameter was then estimated using the model. Extrusion was modeled as one lumped process. The parameters of the ER and mitochondrial handling were taken from the estimates obtained in other intact neurons. The maximal rates of Ca^{2+} fluxes and the concentrations of endogenous buffers were adjusted to reproduce the main characteristics of fluorescence responses measured under voltage-clamp conditions. The same model was able to predict the fluorescence changes during repetitive spike discharge. The effects of the elimination (or addition) of different components of Ca^{2+} transport on the amplitude and half-decay time of simulated fluorescence transients in the digits of GrCs are shown in Fig. 4.

Computational Study of the Distribution of Ca^{2+} Handling Systems in GrCs

Simulation of Ca^{2+} Gradients in Thapsigargin-Treated GrCs

To explore what dendritic specializations may account for spatial gradients of depolarization-induced $[Ca^{2+}]_i$ elevations

in GrCs, we began our simulations from reproducing Ca^{2+} signals in the experimental conditions under which the minimal number of systems contributed to Ca^{2+} handling. At first fluorescence transients obtained after preincubation of cerebellar slices during 30 min with an inhibitor of SERCAs, thapsigargin (TG) [18], were simulated [140]. In these conditions, ER Ca^{2+} transport was abolished, therefore $[Ca^{2+}]_i$ dynamics depended only on Ca^{2+} entry into the cells, diffusion, buffering, extrusion across the PM and the surface-to-volume ratio of cell compartments. However, depolarization-induced Ca^{2+} transients were recorded only in the digits of TG-treated GrCs, and spatial profile of fluorescence change along the dendrite was measured in the absence of TG [18]. Therefore, we examined whether heterogeneities in the distribution of Ca^{2+}-handling systems or cell morphology can account for the smallest $[Ca^{2+}]_i$ gradient, which could be found if CICR occurred only in the digits of GrCs. Our simulations showed that non-uniform distribution of Ca^{2+} pumps or heterogeneities in the fractional volume of the cytosol within the physiological range cannot account for the formation of the Ca^{2+} gradient in GrCs. Instead, Ca^{2+} gradients can be generated by a steep decrease of the calcium current density or an increase in the concentration of fixed endogenous Ca^{2+} buffer(s) in the dendrites of GrCs from their distal to the proximal parts (Fig. 5a–c) [140]. In the latter case, an averaged concentration of the buffer(s) in the parent dendrites should be fairly large, e.g. >400 μM for the buffer with the properties of calretinin, which seems less likely than a non-uniform distribution of Ca^{2+} channels along the dendrite. A simple experiment was proposed to distinguish between the two possibilities (see below).

Evidence for Heterogeneous Distribution of Fixed Endogenous Ca^{2+} Buffers in GrCs

A realistic simulation of cellular calcium dynamics requires not only the reconstruction of the spatiotemporal distribution of $[Ca^{2+}]_i$ rises but also a match of all known experimental and theoretical estimations. To compare I_{Ca} in our model with experimentally measured I_{Ca} [38], calcium currents in all cell compartments were summed together. These currents were obtained with adjusted values of the maximum Ca^{2+} conductance, which allowed us to reproduce the recorded fluorescence changes. Since the time course of fluorescent transient in the soma was not communicated [18], the total I_{Ca} in the model was calculated with the largest physiological value of extrusion rate in this cell compartment [149]. Nevertheless, the calculated peak I_{Ca} in the model with uniformly distributed endogenous buffer appeared to be tens times smaller than the measured peak I_{Ca} [38]. The difference between calculated and experimental currents could not be explained by the presence of endogenous

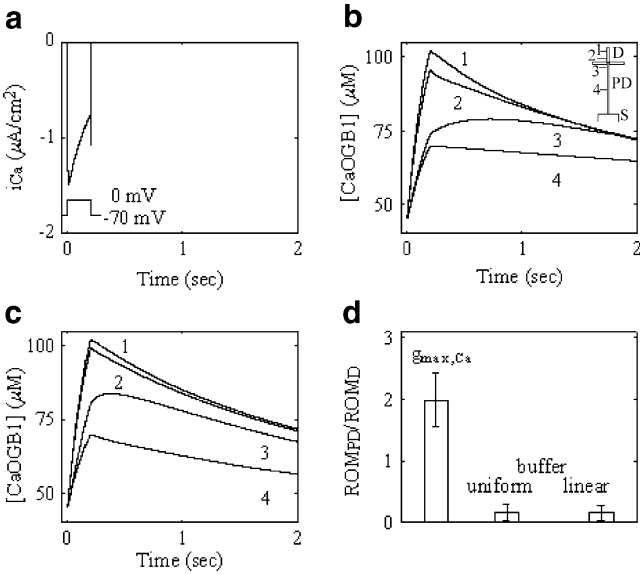

Fig. 5 Spatial heterogeneities that can account for Ca^{2+} gradients in GrCs. **a** Voltage-dependent calcium current in the digits. **b–c** Simulated [CaOGB1] profiles in the digit at locations shown in the inset of **b**. In the *inset*, *D* digit, *PD* parent dendrite and *S* soma. **b** The total concentration of a low-affinity buffer with the dissociation constant 10 μM ($[Buf]_T$) is 0.95 mM in the digits and soma and 18.7 mM in the parent dendrites, respectively. The maximal calcium conductance $g_{max,Ca}=2.0\times10^{-5}$ Scm^{-2} in all cell compartments. **c** In the digits $g_{max,Ca}=1.93\times10^{-5}$ Scm^{-2}, in the parent dendrites $g_{max,Ca}=0.52\times10^{-5}$ Scm^{-2}, $[Buf]_T=0.8$ mM in all cell compartments. **d** The ratio of the half-decay times of fluorescence transients measured with OGB1 and Mag-Fura-2 indicators (ROM) in the middle of the parent dendrite normalized to the value of ROM in the digit (ROM_{PD}/ROM_D). The ratios were determined in the model with inhomogeneous $g_{max,Ca}$ and inhomogeneous distribution of endogenous buffers (which could be uniform or linear in the parent dendrite). *Vertical bars* represent the normalized ROM within the tested ranges of maximum fluorescence change and $[Buf]_T$. If the buffer is distributed uniformly, the ROM is always larger in the parent dendrite than in the digit owing to lower $[Ca^{2+}]_i$ in this cell compartment and the Ca^{2+}-dependence of the OGB1 Ca^{2+} buffer capacity. But if the buffer with a very large buffer capacity is localized in the parent dendrite, the Ca^{2+} buffering is dominated by the endogenous Ca^{2+} buffering capacity. Therefore, the ROM in the parent dendrite is close to 1, whereas the ROM is the digits is expected to be much larger since OGB1 slows significantly the clearance of Ca^{2+} from the cytosol in the digits of GrCs [18]. Adapted from [140] with permission from Elsevier Science. i_{Ca} density of calcium current

buffers with a higher buffer capacity: the half-decay time of fluorescence transients in the digits of GrCs measured with the low-affinity indicator Mag-Fura-2 was much shorter compared to the recordings performed with the high-affinity indicator OGB1 [18] (see also [140]), which indicates that the endogenous buffer capacity in the digits was significantly lower than the total buffer capacity of exogenous and endogenous buffers. After excluding other possibilities, we suggested that some high-capacity immobile Ca^{2+} buffer can be located in the soma of GrCs.

Simulations of NMDAR-mediated Ca^{2+} transients during high-frequency MF stimulation, when GrCs were maintained

at −70 mV in Mg^{2+}-free solution in the presence of mGluR blockers [18], revealed that an estimate of the maximum conductance of NMDARs per digit that was necessary to reproduce fluorescence changes was also at least 8–50-fold lower than the value estimated from the direct measurement of NMDAR-mediated currents in GrCs (Fig. 6a) [140]. An increase in Ca^{2+} extrusion across the PM in the restricted apical part of the digit could not be responsible for this difference; otherwise, the half-decay time of depolarization-induced fluorescence transients in TG-treated cells would be much lower than in the experiment [18]. Then, some immobile buffer was assumed to be highly concentrated immediately underneath the sites where MF–GrC synapses and extrasynaptic NMDARs are situated. Only such localization of the buffer could be reconciled with a pronounced slowing of the decay of depolarization-induced fluorescence responses in the digits of GrCs after introducing a high-affinity Ca^{2+} indicator [140, 150]. Since calretinin makes a prominent contribution to the endogenous buffer capacity of GrCs [19, 90], this buffer was modeled with a fast association rate constant and the apparent dissociation constant of calretinin (1.5 μM) [151]. The largest allowable concentration of a localized buffer with the calretinin properties (16 mM) was calculated as one fifth of the concentration of the densely packed 29 kDa molecules [152]. The simulated changes in the concentration of Ca^{2+}-bound indicator OGB1 ([CaOGB1]) reproduced the peak amplitude and the time course of the experimental fluorescence transients in the digits if 3.6–8 mM of the buffer with five identical Ca^{2+}-binding sites were placed in the most apical compartment of the digits (Fig. 6c). Our simulations showed that, if the fixed Ca^{2+} binding sites were localized only in this cell compartment, the peak amplitude of the I_{Ca} in the model GrCs was 2–7 times smaller than the peak amplitude of the current measured in the experiment. The maximal Ca^{2+} conductance also should be much larger in the apical part than in the rest of the digit. Otherwise, a large Ca^{2+} flux from the part of the digit where the high-affinity buffer is absent to the part where this buffer is highly concentrated would evoke a very rapid decay of fluorescence transient in the middle of the digit [150] that was not observed in experiments. If the buffer with aforementioned properties was placed in the soma and apical parts of the digits, the magnitude of experimental currents could be completely explained [150].

Thus, results of our simulations support the hypothesis that fixed Ca^{2+} buffers and Ca^{2+} channels are very heterogeneously distributed in GrCs.

Ca^{2+}-Binding Proteins in the Models of Calcium Dynamics

The first evidence for a critical role of calretinin in regulating GrC excitability was provided by experiments with calretinin-deficient mice [19]. GrCs from mutant mice have a significantly larger sensitivity to injected depolarizing current, represented by an enhanced increase in AP frequency. Using a phenomenological model of Ca^{2+} dynamics, Gall et al.[19] showed that a fourfold decrease in cytosolic Ca^{2+}-buffering capacity, which was modeled by a constant parameter f in Eq. 1, predicted the increase in the slope of the linear part of current–frequency plot in the cells of calretinin-deficient mice as compared with wild-type controls. When 150 μM BAPTA were infused in the cytosol of GrCs of knockout or wild-type mice in whole-cell recordings, the slope factor was similar to the slope factor measured in the wild-type mice using the perforated patch method. It was suggested that 150 μM BAPTA may mimic the contribution of calretinin to the cytosolic Ca^{2+} buffering

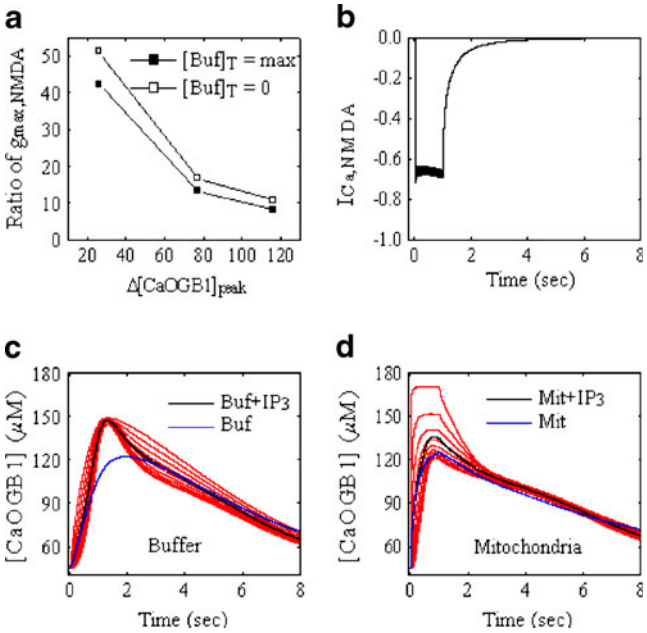

Fig. 6 Simulation of synaptically induced fluorescence transients. **a** The ratio of an estimate of the maximum conductance of NMDARs per digit ($g_{max,NMDA}$) from the direct measurement of NMDAR-mediated currents in GrCs to the $g_{max,NMDA}$ value that was necessary to reproduce the peak values of [CaOGB1] changes (Δ[CaOGB1]$_{peak}$) in our model within the tested ranges of maximum fluorescence change and concentration of uniformly distributed buffer ([Buf]$_T$). **b** Simulation of the calcium current through NMDAR channels in the GrC digit caused by a train of 100 presynaptic stimuli delivered at frequency 100 Hz in Mg^{2+}-free solution at holding membrane potential −70 mV. **c**, **d** [CaOGB1] spatial profiles within the digits of GrCs and [CaOGB1] transients, averaged over the volume of the digits, which were evoked by NMDARs and mGluRs activation. Average [CaOGB1] transients simulated in the presence of mGluR blockers also are shown. **c** The concentration of Ca^{2+} binding sites in the apical part of the digits is 40 mM. **d** Mitochondrial transport with the rate constant of uptake 455.4 ms^{-1} and maximum rate of release 2.1×10^{-4} $mMms^{-1}$ was included in the digits. **a**–**c** Adapted from [140] with permission from Elsevier Science. *Buf* high-capacity buffer in the apical parts of the digits, *Mit* mitochondria in the digits, + *IP*$_3$ IP_3-induced Ca^{2+} release

capacity of GrCs, which controls activation of Ca^{2+}-activated K^+ channels [19]. This assumption implies that an immobile fraction of calretinin is very low in GrCs. However, there are several evidences that other Ca^{2+}-handling processes can compensate for absent calretinin in GrCs. After a selective reexpression of genuine calretinin in GrCs of transgenic mice, normal GrC excitability was restored, but these cells contained 80-fold less calretinin than in wild-type mice [96]. Another study demonstrated a strong spike frequency accommodation in wild-type GrCs studied in whole-cell recordings with low BAPTA; such an accommodation was absent in the perforated patch recordings from calretinin-deficient GrCs [19]. In both studies, compensatory mechanisms were suggested to account for the observations in mutants. For this reason it would be possible to assume only that the Ca^{2+} buffering speed of mobile calretinin in GrCs is similar to that of 150 μM BAPTA. However, BAPTA and calretinin have very different kinetics of Ca^{2+} binding (fast and cooperative), diffusion constants, and occupancy by Ca^{2+} at any initial $[Ca^{2+}]_i$ [94]. Therefore, their Ca^{2+} buffer capacity cannot be similar under different experimental conditions, e.g. at different current intensities. Alternatively, almost indistinguishable current–frequency plots obtained with conventional whole-cell and perforated patch recordings [19, 131] may result from the same Ca^{2+} levels within Ca^{2+} nano/microdomains sensed by BK_{Ca} channels in the presence of both buffers.

BK_{Ca} channels in GrCs are activated during the short duration of an AP, with a half-width of <1 ms and produce a fast afterhyperpolarization [137]. This suggests that BK_{Ca} channels in GrCs probably form fast-activating complexes with N-type Ca^{2+} channels [139]. Based upon simulations of similar effects of BAPTA and calretinin on Ca^{2+} diffusion nearby a single Ca^{2+} channel or a large cluster of Ca^{2+} channels, we estimated the concentration of mobile calretinin in GrCs of 1.2 and 0.7 mM, respectively (E. Saftenku, unpublished observations). At first sight, a high concentration of calretinin cannot be reconciled with low endogenous buffer capacity of ~56 in presynaptic terminals of GrCs. This estimate was obtained from a plot of the inverse of the peak amplitudes of AP-evoked $[Ca^{2+}]_i$ transients versus added buffer capacity [116]. However, an essential property of calretinin, which has not been paid attention previously, is a very delayed equilibration with Ca^{2+} due to the competition for Ca^{2+} between Ca^{2+}-binding sites with different kinetics. Our simulations show that, because of its binding properties, calretinin binds Ca^{2+} much less effectively during brief APs than during slower Ca^{2+} influx or trains of APs. Thus, the relationship between the inverse of the calcium peak and added buffer capacity in [116] can be accurately reproduced in the presence of 1.2 mM calretinin as the sole buffer in the model (E. Saftenku, unpublished observations).

In our modeling study [140], the experimental data of Gall et al. [18] performed under conditions where mobile endogenous buffers were washed-out during whole-cell recordings were explained by a high concentration of fixed Ca^{2+}-binding sites in the apical parts of GrC digits and in the soma. It was suggested that the buffer that possesses these Ca^{2+}-binding sites could be membrane-associated calretinin. Although the localization of immobilized calretinin in GrCs can be proven only using immunohistochemical techniques, several observations suggest this may be the case. Firstly, calretinin can be highly concentrated beneath the PM in other neurons, for example, in brainstem auditory neurons with the formation of mature synapses [153]. Secondly, 10–27% of calretinin in the adult rat cerebellum was found to be associated with membrane fractions [154, 155] where it was most abundant in the synaptic membrane (up to 50% from cytosolic fraction) [155]. It is known that calretinin may change its expression and localization during development [90, 153], but there is no evidence that such changes occur after GrC maturation. Thirdly, a theoretical estimate of the concentration of immobilized calretinin in the apical part of the digits [140] corresponds to 60–165 μM of calretinin after its averaging over the entire cell volume. A similar estimate was obtained when calretinin was modeled with cooperative Ca^{2+} binding kinetics (E. Saftenku, unpublished observations). These values are in a good agreement with our estimates of mobile calretinin in GrCs (see above). In contrast, a very large concentration of immobilized calretinin in the soma [140, 150] does not seem likely.

Other identified endogenous buffers cannot be responsible for much lower amplitudes of Ca^{2+} transients [18] than expected from typical measurements of Ca^{2+} and NMDAR currents in whole-cell recordings. Calmodulin has two pairs of cooperative Ca^{2+} binding sites with lower affinities than calretinin (with the apparent K_d around 4 and 17 μM [156]). Assuming the commonly used calmodulin concentration (10 μM [157]), the experimentally determined fraction of an immobilized calmodulin in Purkinje cells (20% [158]), and the lower levels of calmodulin expression in GrCs than in Purkinje cells [97], calmodulin concentration in the apical parts of the GrC digits can be predicted to be not more than 100 μM, which is much lower than the estimates of calretinin concentration in our model [140]. NCS-1 was found in the brain at concentrations of 0.5–5 μM [159]. This buffer is constitutively associated with the PM and the trans-Golgi network [99]. Apart from NCS-1, only NVP-1 can be found in the membrane fraction of rat GrCs even at resting $[Ca^{2+}]_i$ [160] and therefore is not washed out in whole-cell recordings. NVP-1 exhibits cooperative Ca^{2+} binding with much lower affinity than calretinin (5.8 μM [161]), whereas NCS-1 has one pair of cooperative Ca^{2+}-binding sites with the apparent $K_d \approx$

1.8 μM and an independent Ca^{2+}-binding site with the $K_d \approx$ 0.4 μM [162]. If even the latter buffer was taken at the largest estimated concentration and completely placed to the apical parts of the digits or to the soma of our model GrC [140], the simulated $[Ca^{2+}]_i$ transients were decreased only by 30% and 1%, respectively. These results indicate that although calcium sensor proteins can contribute to the cytosolic endogenous Ca^{2+} binding capacity of GrCs, their contribution is likely to be minor. It cannot be excluded that some other unidentified high-capacity buffer is localized in the soma of GrCs. Otherwise, the discrepancy between the characteristics of experimentally measured and simulated depolarization-induced I_{Ca} are likely to be explained by experimental errors or insufficient statistics.

The functional consequences of localization of Ca^{2+}-binding sites in the apical part of the digits could be an adaptation to large calcium influxes through NMDAR-mediated channels. In vivo studies show that the cerebellar MF terminal can fire at over 200 Hz for sustained periods [163], and sustained vesicular release at high rates is preserved at each release site of MF to GrC synapse [24]. The association of calretinin with the PM would attenuate large $[Ca^{2+}]_i$ responses and result in more compressed Ca^{2+} gradients as compared with the uniformly distributed buffer (Fig. 7). Conversely, Ca^{2+} microdomains evoked by Ca^{2+} release from the ER would be relatively unaffected by the buffers that are associated with the PM. This can partially explain why the induction of long-term depression at MF−GrC synapses by low-frequency presynaptic stimulation, which is determined by the level of postsynaptic $[Ca^{2+}]_i$, requires activation of mGluRs but does not require activation of NMDARs [164]. Localization of a high-capacity buffer in the soma may serve the same function of preventing Ca^{2+} overload in pathological conditions associated with excitotoxicity. This is possible because NMDARs are readily detected in somatic patches from GrCs in slices [165], and the density of NMDARs in the soma of cultured GrCs is likely to be even higher than in neurites [119].

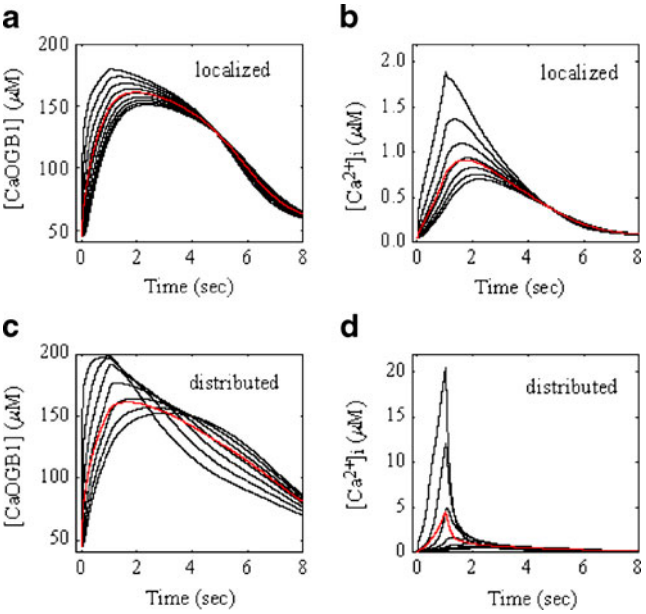

Fig. 7 Effect of spatial buffer localization in the digits of GrCs. [CaOGB1] (**a**, **c**) and $[Ca^{2+}]_i$ (**b**, **d**) spatial profiles within the digits (*thin lines*) and average transients (*bold lines*) initiated by NMDAR-mediated calcium influx in response to 1 s presynaptic stimulation of mossy fibers with frequency 100 Hz in Mg^{2+}-free solution in the presence of mGluR blockers are shown. The simulations are carried out for the maximum fluorescence change of 0.4. **a**, **b** Calretinin is localized in the apical part of the digit of 0.5 μm length in concentration of 3.8 mM. **c**, **d** The same amount of calretinin is uniformly distributed throughout the digit in concentration of 0.42 mM. The maximum rate of extrusion ($v_{max,PM}$) is 108 pmol $(cm^2 s)^{-1}$ in the apical part of the digit and 1.25 pmol $(cm^2 s)^{-1}$ in the rest of the digit and in the parent dendrite. Other parameters are as in [140]

Mitochondrial and ER Transport

To study the role of mitochondria in shaping Ca^{2+} transients in GrCs, we used a quantitative description of the dependence of mitochondrial transport on $[Ca^{2+}]_i$ derived for sympathetic neurons [166]. The results of simulations [140] showed that mitochondrial Ca^{2+} uptake scarcely influenced $[Ca^{2+}]_i$ changes evoked by 200 ms depolarization, but it could decrease the $[Ca^{2+}]_i$ elevations induced by high-frequency synaptic stimulation (Fig. 6d). These findings are in agreement with recent studies in hippocampal dendrites showing that mitochondrial calcium fluxes are stimulated by cytosolic Ca^{2+} levels of above 500–600 nM and that mitochondrial Ca^{2+} uptake occurs rapidly in response to synaptically evoked Ca^{2+} transients [167]. Therefore, Ca^{2+} uptake by mitochondria might explain lower $[Ca^{2+}]_i$ transients than expected from typical measurements of NMDAR-mediated current. However, simulated [CaOGB1] changes evoked by NMDAR activation in the presence of mGluR blockers had almost 2-fold lower time to peak than in the experiment [18]. Moreover, inclusion of IICR in the model resulted in a lower increase in the peak amplitude of [CaOGB1] transient (6–11 versus 25%) and a more prominent Ca^{2+} gradient along the digits than in the experiment [18] and in the model with the localized buffer (Fig. 6c, d). If a high-capacity endogenous buffer was located in the apical part of the digits, mitochondria had only a small additive influence on the amplitude of calcium transients. The assumption that CICR contributes to synaptically induced calcium transients and is significantly enhanced by IICR can partly explain the discrepancy between the simulations and experiments. It is more difficult to explain a low Ca^{2+} gradient along the

digit, and more experiments with larger statistics are needed to make any predictions.

In the experiments of Gall et al. [18], CICR amplified an initial depolarization-induced Ca^{2+} signal in the digits of GrCs by 1.4-fold [18]. Regenerative CICR, i.e., self-reinforcing CICR after termination of external Ca^{2+} entry, is rarely observed in neurons in the absence of caffeine [57]. Its mechanisms in central neurons are not yet well understood since direct measurements of luminal calcium in these cells have only recently begun [168]. Our preliminary simulations based on the interplay between fluxes across the ER and PM, with decrease of the driving force for passive Ca^{2+} release from the ER as the sole mechanism of CICR termination, could reproduce the main experimental observations in GrCs. This finding is consistent with the experimental results of Albrecht et al. [169] in peripheral sympathetic neurons. When ER transport was added to the model only to the digit compartment, the spatial profiles of experimental fluorescence and simulated [CaOGB1] changes were in close agreement (Fig. 3b) [140], suggesting that the density of the ER is much lower in the parent dendrites and soma than in the digits of GrCs. The best fit to the experimental normalized amplitudes of fluorescence transients evoked by synaptic stimulation at different distances from the soma (Fig. 3b) was also obtained when IICR was confined to the digits of GrCs [140]. The involvement of CICR or SERCA in the depolarization-induced $[Ca^{2+}]_i$ transients in the soma of GrCs was not observed in slices of mouse [55] and in rat culture [48], supporting the hypothesis about the ER distribution.

Future Directions

Model Predictions and Their Verification

The computational analysis of $[Ca^{2+}]_i$ measurements in GrCs resulted in two main hypotheses. First, in order to explain depolarization-induced Ca^{2+} gradients in GrCs, the density of Ca^{2+} channels should decrease, or the concentration of some fixed endogenous Ca^{2+} buffers should increase from the digits toward the soma. It is likely that the ER is also heterogeneously distributed in GrC dendrites. These predictions can be tested experimentally. The ER can be visualized with ER-Tracker dyes and confocal microscopy [170]. The distribution of various subtypes of Ca^{2+} channels can be studied using cell-attached or outside-out patch techniques [171] together with nanopipettes of submicron diameter [172] or two-photon imaging techniques together with statistical analysis of signal fluctuations [173]. Both approaches are very challenging, but immunogold methods and light microscope immunohistochemistry also can be useful for studying the distribution of specific subunits of Ca^{2+} channels, e.g., [174, 175]. In addition, we proposed a simple experiment [140] to distinguish between the heterogeneous distribution of Ca^{2+} current density and endogenous buffers along the GrC dendrite. For this, fluorescence transients in both parent dendrites and digits can be recorded using two indicator dyes with different affinities to Ca^{2+} ions under conditions when Ca^{2+} uptake and release by internal stores are inhibited (Fig. 5d). Second, the most plausible hypothesis that explains much slower $[Ca^{2+}]_i$ changes in the model than expected from depolarization and synaptically induced Ca^{2+} currents, typically measured in GrCs after the formation of mature synapses, is a high localization of immobile calretinin in the apical parts of GrC digits. We also used simulations to estimate the concentration of mobile calretinin in GrCs in the order of 1 mM. Our hypotheses and estimations can be evaluated using immunofluorescence labeling of calretinin and other identified endogenous buffers in cerebellar slices [153] in combination with supraresolution two-photon laser scanning microscopy [2] and quantitative immunogold labeling together with electron microscopy [176]. A fraction of immobilized calretinin in the different parts of the cell can be estimated from fluorescence recovery after photobleaching of fluorescently tagged recombinant calretinin [151, 177]. Theoretically, mitochondria also may influence the amplitude of synaptically evoked Ca^{2+} transients, but this influence is expected to be negligible in the presence of a high-capacity endogenous buffer. Our simulations predict that an observation of a significant delay in the time to peak of fluorescence transient in the digit after termination of synaptic stimulation in the recordings performed in the presence of mGluR blockers and TG indicates the presence of some high-capacity buffer. The existence of such a delay can be established experimentally.

A Framework for Characterization of Ca^{2+} Handling in GrCs

Our model [140] is only the first step towards understanding the role of Ca^{2+} handling in GrC physiology. For its further refinement, the following framework can be suggested, which builds on previous work in sympathetic neurons [148]. Fluorescence measurements in GrCs can be made under experimental conditions where all but a few transport pathways are blocked, with further addition of other Ca^{2+} handling mechanisms and reconstruction of Ca^{2+} dynamics step by step using simulations. Then, the relevant importance of the distribution of different Ca^{2+} handling systems for localization of Ca^{2+} responses can be investigated, and a number of experimentally inaccessible parameters, such as spatiotemporal characteristics of Ca^{2+} signals in unperturbed neurons and the IP_3 concentration, can be estimated. An

exact distribution of all receptors and transporters, necessary for a refined model development, should be studied using quantitative electron microscopic analysis of pre-embedding immunogold reactions in cerebellar sections [178]. However, the spatial density of Ca^{2+} channels, transporters, fixed buffers, mitochondrial uniporters, and RyRs can be preliminary estimated or specified with the model. Identified critical Ca^{2+} handling mechanisms can then be subjected to more detailed experimental analysis.

Important requirements for further $[Ca^{2+}]_i$ measurements are the determination of the $(\Delta F/F)_{max}$ using extrapolation to the true value [179] and avoiding the problems with incorrect determination of background fluorescence [180]. At first, synaptically and depolarization-induced Ca^{2+} transients can be measured after pretreatment with the inhibitors of Ca^{2+} uptake by mitochondria and the ER and in the presence of blockers of PMCA (e.g., carboxyeosin [181]) or specific inhibitors of Na^+–Ca^{2+} exchangers. It may be useful to examine preliminarily if the inhibitors of SERCA, mitochondrial calcium transport, and SOC entry influence glutamate release at MF−GrC synapses, e.g. sensitivity of presynaptic depression to these drugs. If so, NMDAR-mediated currents should be measured each time when these drugs are applied. To account for SOC entry [69], all experiments are to be performed, at least initially, in the presence of selective SOC channel antagonists, e.g. MRS 1845 [71]. After obtaining information about the distribution and relative concentration of different identified fixed endogenous buffers and transporters in GrCs, the following strategy can be used. To account for unidentified endogenous buffers in GrCs, the sets of the best fits of parameters that reproduce synaptically evoked Ca^{2+} transients with different concentrations of low-affinity buffers can be found. Then the spatial density of calcium current can be estimated from the fit of depolarization-induced Ca^{2+} transients, and the ratios of the decay times of these transients can be calculated in the presence of two exogenous buffers with different affinities, e.g. OGB1 and Mag-Fura-2, and compared with the experimental ratios. The stimuli with different amplitude and duration can be used to specify the Michaelis constants of two extrusion systems.

Because ATP production may exert local control on SERCA activity [182], the contribution of mitochondrial transport to evoked Ca^{2+} transients is expected to be studied before the contribution of ER transport. For this, $[Ca^{2+}]_i$ transients in the absence and presence of inhibitors of mitochondrial uniporter are to be compared in TG-treated GrCs. Mitochondrial Ca^{2+} uptake can be described in the presence of the inhibitor of mitochondrial Na^+-Ca^{2+} exchanger. However, it should be taken into account that a commonly used drug CGP 37157 blocks Na^+-Ca^{2+}-exchange not only in mitochondria of GrCs, but also in the PM [183]. Mitochondrial Ca^{2+} concentration can be measured in slices simultaneously with cytosolic Ca^{2+} concentration using fluorescence dyes, e.g. the AM form of rhod-2 [184], although these dyes can underestimate intramitochondrial concentrations [185]. An additional difficulty in the study of the fast mitochondrial Ca^{2+} uptake is its dependence on presumed high-Ca^{2+} microdomains on the close apposition between mitochondria and the sites of Ca^{2+} release/influx [186]; therefore, more complex models combining a detailed model of a microdomain coupled with a model of entire cell [187] may be necessary for adequate description of mitochondrial Ca^{2+} transport.

The parameters of Ca^{2+} uptake by the ER can be specified by simulations of measured $[Ca^{2+}]_i$ elevations after rapid SERCA inhibition at different times during their recovery phase (for details of the experiment see [188]). Then, the model parameters of CICR can be estimated by comparison of experiments and simulations in the absence of any inhibitors (besides of mGluR blockers in the case of synaptically evoked Ca^{2+} transients). To account for mechanisms that terminate the Ca^{2+} release from the ER, further investigations of the dependence of the rate of Ca^{2+} uptake and the permeability of the ER on intraluminal Ca^{2+} concentration and time are needed. Nowadays, AM-ester loading of low-affinity dyes in combination with patch-pipette dialysis and simultaneous imaging of Ca^{2+} dynamics in the ER by a low-affinity dye and in the cytosol by a high-affinity dye, probably, is the most appropriate for the cells studied in slices [168]. Measurements of Ca^{2+} concentration in the ER and mitochondria in GrCs under physiological conditions in vivo [168, 189] using genetically encoded Ca^{2+} indicators seem to be particularly promising for the future. At last heparin, a blocker of IP_3 receptors, can be applied to check if group-I mGluRs can mobilize intracellular Ca^{2+} not only through IP_3 receptors, but also through RyRs as it was shown in developing cultures [67].

In such a manner, a complete system of Ca^{2+} handling in GrCs may be characterized via the interaction of experiment and model development.

Conclusions

The experimental findings reveal spatial compartmentalization and heterogeneity in Ca^{2+} signaling within dendrites of cerebellar GrCs and significant influence of calretinin on GrC intrinsic excitability. Mathematical models are a helpful means to test whether the specific distribution and interplay between proposed Ca^{2+} transport systems can explain the spatiotemporal dynamics of measured Ca^{2+} responses. Being, in essence, a collection of hypotheses, models are most useful when their predictions fail to match experiments. Having excluded several other possibilities, we elaborated the most plausible hypothesis of a highly uneven distribution of

immobile endogenous buffer(s) and presumably Ca^{2+} channels in cerebellar GrCs. Moreover, we developed an approach that can be applied for theoretical study of calcium dynamics that underlies spatially non-uniform Ca^{2+} responses. All components of this approach are equally important when simulations are performed under conditions of incomplete experimental data. The predictions of the model can be tested experimentally. One outcome of computational analysis is an improved understanding of the critical determinants of Ca^{2+} signal generation and identification of critical Ca^{2+} handling mechanisms for more detailed experimental analysis. For further refinements of the model, a plan of step-by-step reconstruction of spatially nonuniform Ca^{2+} responses through new experiments combined with simulations is described. A similar approach can be used to investigate Ca^{2+} dynamics in other cells. Ultimately, a deep understanding of calcium dynamics will be required for rational treatments of pathologies in calcium regulation.

Acknowledgements I would like to thank sincerely David Friel for helpful comments and constant support and Thomas Nielsen for help with editing.

Conflict of Interest Statement I declare that the research was conducted in the absence of any commercial or financial relationships that could be construed as a potential conflict of interest.

References

1. Iyer V, Hoogland TM, Saggau P. Fast functional imaging of single neurons using random-access multiphoton (RAMP) microscopy. J Neurophysiol. 2006;95:535–45.
2. Ding JB, Takasaki KT, Sabatini BL. Supraresolution imaging in brain slices using stimulated-emission depletion 2-photon laser scanning microscopy. Neuron. 2009;63:429–37.
3. Wallace DJ, Meyer zum Alten Borgloh S, Astori S, Yang Y, Bausen M, Kügler S, et al. Single-spike detection in vitro and in vivo with a genetic Ca^{2+} sensor. Nat Meth. 2008;5:797–804.
4. Grewe BF, Helmchen F. Optical probing of neuronal ensemble activity. Curr Opin Neurobiol. 2009;19:520–9.
5. Tour O, Adams SR, Kerr RA, Meijer RM, Sejnowski TJ, Tsien RW, et al. Calcium Green FlAsH as a genetically targeted small-molecule calcium indicator. Nat Chem Biol. 2007;3:423–31.
6. Higley MJ, Sabatini BL. Calcium signaling in dendrites and spines: practical and functional considerations. Neuron. 2008;59:902–13.
7. Augustine GJ, Santamaria F, Tanaka K. Local calcium signaling in neurons. Neuron. 2003;40:331–46.
8. Rizzuto R, Pozzan T. Microdomains of intracellular Ca^{2+}: molecular determinants and functional consequences. Physiol Rev. 2006;86:369–408.
9. Friel DD, Chiel HJ. Calcium dynamics: analyzing the Ca^{2+} regulatory network in intact cells. Trends Neurosci. 2008;31:8–19.
10. Herculano-Houzel S, Lent R. Isotropic fractionator: a simple, rapid method for the quantification of total cell numbers in the brain. J Neurosci. 2005;25:2518–21.
11. Azevedo FA, Carvalho LR, Grinberg LT, Farfel JM, Ferretti RE, Leite RE, et al. Equal numbers of neuronal and nonneuronal cells make the human brain an isometrically scaled-up primate brain. J Comp Neurol. 2009;513:532–41.
12. Andersen BB, Gundersen HJ, Pakkenberg B. Aging of the human cerebellum: a stereological study. J Comp Neurol. 2003;466:356–65.
13. Pelvig DP, Pakkenberg H, Stark AK, Pakkenberg B. Neocortical glial cell numbers in human brains. Neurobiol Aging. 2008;29:1754–62.
14. Sato M, Suzuki K, Yamazaki H, Nakanishi S. A pivotal role of calcineurin signaling in development and maturation of postnatal cerebellar granule cells. Proc Natl Acad Sci USA. 2005;102:5874–9.
15. Nakanishi S, Okazawa M. Membrane potential-regulated Ca^{2+} signalling in development and maturation of mammalian cerebellar granule cells. J Physiol. 2006;575(Pt 2):389–95.
16. Mintz IM, Sabatini BL, Regehr WG. Calcium control of transmitter release at a cerebellar synapse. Neuron. 1995;15:675–88.
17. Atluri PP, Regehr WG. Determinants of the time course of facilitation at the granule cell to Purkinje cell synapse. J Neurosci. 1996;16:5661–71.
18. Gall D, Prestori F, Sola E, D'Errico A, Roussel C, Forti L, et al. Intracellular calcium regulation by burst discharge determines bidirectional long-term synaptic plasticity at the cerebellum input stage. J Neurosci. 2005;25:4813–22.
19. Gall D, Roussel C, Susa I, D'Angelo E, Rossi P, Bearzatto B, et al. Altered neuronal excitability in cerebellar granule cells of mice lacking calretinin. J Neurosci. 2003;23:9320–7.
20. Budd SL, Nicholls DG. Mitochondria, calcium regulation, and acute glutamate excitotoxicity in cultured cerebellar granule cells. J Neurochem. 1996;67:2282–91.
21. Bawa B, Abbott LC. Analysis of calcium ion homeostasis and mitochondrial function in cerebellar granule cells of adult CaV 2.1 calcium ion channel mutant mice. Neurotox Res. 2008;13:1–18.
22. Contestabile A. Cerebellar granule cells as a model to study mechanisms of neuronal apoptosis or survival in vivo and in vitro. Cerebellum. 2002;1:41–55.
23. Mugnaini E. The histology and cytology of the cerebellar cortex. In: Larsell O, Jansen J, editors. Comparative anatomy and histology of the cerebellum. The human cerebellum, cerebellar connections and cerebellar cortex. Minneapolis: The University of Minnesota Press; 1972. p. 201–51.
24. Saviane C, Silver RA. Fast vesicle reloading and a large pool sustain high bandwidth transmission at a central synapse. Nature. 2006;439:983–7.
25. Chadderton P, Margrie TW, Häusser M. Integration of quanta in cerebellar granule cells during sensory processing. Nature. 2004;428:856–60.
26. Jörntell H, Ekerot CF. Properties of somatosensory synaptic integration in cerebellar granule calls in vivo. J Neurosci. 2006;26:11786–97.
27. Palay SL, Chan-Palay V. Cerebellar cortex. Berlin: Springer; 1974.
28. Jakab RL, Hámori J. Quantitative morphology and synaptology of cerebellar glomeruli in rat. Anat Embryol (Berl). 1988;179:81–8.
29. Cathala L, Brickley S, Cull-Candy S, Farrant M. Maturation of EPSCs and intrinsic membrane properties enhances precision at a cerebellar synapse. J Neurosci. 2003;23:6074–85.
30. Cathala L, Holderith NB, Nusser Z, DiGregorio DA, Cull-Candy SG. Changes in synaptic structure underlie the developmental speeding of AMPA receptor-mediated EPSCs. Nat Neurosci. 2005;8:1310–8.
31. Sommer B, Köhler M, Sprengel R, Seeburg PH. RNA editing in brain controls a determinant of ion flow in glutamate-gated channels. Cell. 1991;67:11–9.

32. Longone P, Impagnatiello F, Mienville JM, Costa E, Guidotti A. Changes in AMPA receptor-spliced variant expression and shift in AMPA receptor spontaneous desensitization pharmacology during cerebellar granule cell maturation in vitro. J Mol Neurosci. 1998;11:23–41.
33. Cull-Candy S, Kelly L, Farrant M. Regulation of Ca^{2+}-permeable AMPA receptors: synaptic plasticity and beyond. Curr Opin Neurobiol. 2006;16:288–97.
34. Smith TC, Wang LY, Howe JR. Distinct kainate receptor phenotypes in immature and mature mouse cerebellar granule cells. J Physiol. 1999;517(Pt 1):51–8.
35. DiGregorio DA, Nusser Z, Silver RA. Spillover of glutamate onto synaptic AMPA receptors enhances fast transmission at a cerebellar synapse. Neuron. 2002;35:521–33.
36. Burnashev N, Zhou Z, Neher E, Sakmann B. Fractional calcium currents through recombinant GluR channels of the NMDA, AMPA and kainite receptor subtypes. J Physiol. 1995;485:403–18.
37. Randall A, Tsien RW. Pharmacological dissection of multiple types of Ca^{2+} channel currents in rat cerebellar granule neurons. J Neruosci. 1995;15:2995–3012.
38. Rossi P, D'Angelo E, Magistretti J, Toselli M, Taglietti V. Age-dependent expression of high-voltage activated calcium currents during cerebellar granule cell development in situ. Pflügers Arch. 1994;429:107–16.
39. Brown SP, Safo PK, Regehr WD. Endocannabinoids inhibit transmission at granule cell to Purkinje cell synapses by modulating three types of presynaptic calcium channels. J Neurosci. 2004;24:5623–31.
40. Kulik A, Nakadate K, Hagiwara A, Fukazawa Y, Luján R, Saito H, et al. Immunocytochemical localization of the α1A subunit of the P/Q-type calcium channel in the rat cerebellum. Eur J Neurosci. 2004;19:2169–78.
41. Bawa B, Abbott LC. Alterations in intracellular calcium ion concentrations in cerebellar granule cells of the CACNA1A mutant mouse, leaner, during postnatal development. Neurotox Res 2009; in press.
42. Guerini D, Coletto L, Carafoli E. Exporting calcium from cells. Cell Calcium. 2005;38:281–9.
43. Kiedrowski L, Czyż A, Baranauskas G, Li XF, Lytton J. Differential contribution of plasmalemmal Na^{+}/Ca^{2+} exchange isoforms to sodium-dependent calcium influx and NMDA excitotoxicity in depolarized neurons. J Neurochem. 2004;90:117–28.
44. Guerini D, Garcia-Martin E, Gerber A, Volbracht C, Leist M, Merino CG, et al. The expression of plasma membrane Ca^{2+} pump isoforms in cerebellar granule neurons is modulated by Ca^{2+}. J Biol Chem. 1999;273:1667–76.
45. Marcos D, Sepulveda MR, Berrocal M, Mata AM. Ontogeny of ATP hydrolysis and isoform expression of the plasma membrane Ca^{2+}-ATPase in mouse brain. BMC Neurosci. 2009;10:112.
46. Hillman DE, Chen S, Bing R, Penniston JT, Llinas R. Ultrastuctural localization of the plasmalemmal calcium pump in cerebellar neurons. Neuroscience. 1996;72:315–24.
47. Burette AC, Strehler EE, Weinberg RJ. "Fast" plasma membrane calcium pump PMCA2a concentrates in GABAergic terminals in the adult rat brain. J Comp Neurol. 2009;512:500–13.
48. Ivannikov MV, Sugimori H, Llinas RR. Calcium clearance and its energy requirements in cerebellar neurons. Cell Calcium. 2010;47:507–13.
49. Visser F, Lytton J. K^{+}-dependent Na^{+}/Ca^{2+} exchangers: key contributors to Ca^{2+} signaling. Physiology (Bethesda). 2007;22:185–92.
50. Seil FJ, Herndon RM. Cerebellar granule cells in vitro. A light and electron microscope study. J Cell Biol. 1970;45:212–20.
51. Hajós F, Kerpel-Fronius S. Electron microscope histochemical evidence for a partial or total block of the tricarboxylic acid cycle in the mitochondria of presynaptic axon terminals. J Cell Biol. 1971;51:216–22.
52. Fiala JC, Harris KM. Dendrite structure. In: Stuart G, Spruston N, Häusser M, editors. Dendrites. Oxford: Oxford University Press; 1999. p. 1–34.
53. Irving AJ, Collingridge GL, Schofield JG. Interactions between Ca^{2+} mobilizing mechanisms in cultured rat cerebellar granule cells. J Physiol. 1992;456:667–80.
54. Simpson PB, Nahorski SR, Challiss RA. Agonist-evoked Ca2+ mobilization from stores expressing inositol 1, 4, 5-trisphosphate receptors and ryanodine receptors in cerebellar granule neurones. J Neurochem. 1996;67:363–73.
55. Kirischuk S, Voitenko N, Kostyuk P, Verkhratsky A. Calcium signalling in granule neurones studied in cerebellar slices. Cell Calcium. 1996;19:59–71.
56. Aronica E, Nicoletti F, Condorelli DF, Balázs R. Pharmacological characterization of metabotropic glutamate receptors in cultured cerebellar granule cells. Neurochem Res. 1993;18:605–12.
57. Verkhratsky A. Physiology and pathophysiology of the calcium store in the endoplasmic reticulum of neurons. Physiol Rev. 2005;85:201–79.
58. del Río E, McLaughlin M, Downes CP, Nicholls DG. Differential coupling of G-protein-linked receptors to Ca2+ mobilization through inositol(1, 4, 5)trisphosphate or ryanodine receptors in cerebellar granule cells in primary culture. Eur J Neurosci. 1999;11:3015–22.
59. Masgrau R, Servitja JM, Young KW, Pardo R, Sarri E, Nahorski SR, et al. Characterization of the metabotropic glutamate receptors mediating phospholipase C activation and calcium release in cerebellar granule cells: calcium-dependence of the phospholipase C response. Eur J Neurosci. 2001;13:248–56.
60. Berthele A, Laurie DJ, Platzer S, Zieglgänsberg W, Tölle TR, Sommer B. Differential expression of rat and human type I metabotropic glutamate receptor splice variant messenger RNAs. Neuroscience. 1998;85:733–49.
61. Takemura M, Kitanaka N, Kitanaka J. Signal transduction by histamine in the cerebellum and its modulation by N-methyltransferase. Cerebellum. 2003;2:39–43.
62. Schambra UB, Mackensen GB, Stafford-Smith M, Haines DE, Schwinn DA. Neuron specific alpha-adrenergic receptor expression in human cerebellum: implications for emerging cerebellar roles in neurologic disease. Neuroscience. 2005;135:507–23.
63. Takayasu Y, Iino M, Furuya N, Ozawa S. Muscarine-induced increase in frequency of spontaneous EPSCs in Purkinje cells in the vestibulo-cerebellum of the rat. J Neurosci. 2003;23:6200–8.
64. Baude A, Nusser Z, Robers JD, Mulvihill E, McIlhinney RA, Somagyi P. The metabotropic glutamate receptor (mGluR1α) is concentrated at perisynaptic membrane of neuronal subpopulations detected by immunogold reaction. Neuron. 1993;11:771–87.
65. Furuichi T, Furutama D, Hakamata Y, Nakai J, Tekeshima H, Mikoshiba K. Multiple types of ryanodine receptor/Ca^{2+} release channels are differentially expressed in rabbit brain. J Neurosci. 1994;14:4794–805.
66. Sammels E, Parys JB, Missiaen L, De Smedt H, Bultynck G. Intracellular Ca^{2+} storage in health and disease: a dynamic equilibrium. Cell Calcium. 2010;47:297–314.
67. Fagni L, Chavis P, Ango F, Bockaert J. Complex interactions between mGluRs, intracellular Ca^{2+} stores and ion channels in neurons. Trends Neurosci. 2000;23:80–8.
68. Krause KH, Michalak M. Calreticulin. Cell. 1997;88:439–43.
69. Singaravelu K, Lohr C, Deitmer JW. Calcium-independent phospholipase A2 mediates store-operated calcium entry in rat cerebellar granule cells. Cerebellum. 2008;7:467–81.
70. Pinilla PJ, Hernandez AT, Camello MC, Pozo MJ, Toescu EC, Camello PJ. Non-stimulated Ca^{2+} leak pathway in cerebellar granule neurones. Biochem Pharmacol. 2005;70:786–93.

71. Szikra T, Cusato K, Thoreson WB, Barabas P, Bartoletti TM, Krizaj D. Depletion of calcium stores regulates calcium influx and signal transmission in rod photoreceptors. J Physiol. 2008;586(Pt 20):4859–75.
72. Baba A, Yasui T, Fujisawa S, Yamada RX, Yamada MK, Nishiyama N, et al. Activity-evoked capacitative Ca^{2+} entry: implications in synaptic plasticity. J Neurosci. 2003;23:7737–41.
73. Roos J, DiGregorio PJ, Yeromin AV, Ohlsen K, Lioudyno M, Zhang S, et al. STIM1, an essential and conserved component of store-operated Ca^{2+} channel function. J Cell Biol. 2005;169:435–45.
74. Brandman O, Liou J, Park WS, Meyer T. STIM2 is a feedback regulator that stabilizes basal cytosolic and endoplasmic reticulum Ca^{2+} levels. Cell. 2007;131:1327–39.
75. Skibinska-Kijek A, Wisniewska MB, Gruszczynska-Biegala J, Methner A, Kuznicki J. Immunolocalization of STIM1 in the mouse brain. Acta Neurobiol Exp (Wars). 2009;69:413–28.
76. Celsi F, Pizzo P, Brini M, Leo S, Fotino G, Pinton P, et al. Mitochondria, calcium and cell death: a deady triad in neurodegeneration. Biochim Biophys Acta. 2009;1787:335–44.
77. Gunter TE, Pfeiffer DR. Mechanisms by which mitochondria transport calcium. Am J Physiol. 1990;258:C755–86.
78. Colegrove SL, Albrecht MA, Friel DD. Dissection of mitochondrial Ca^{2+} uptake and release fluxes in situ after depolarization-evoked $[Ca^{2+}]_i$ elevations in sympathetic neurons. J Gen Physiol. 2000;115:351–70.
79. Ankarcrona M, Dypbukt JM, Bonfoco E, Zhivotovsky B, Orrenius S, Lipton SA, et al. Glutamate-induced neuronal death: a succession of necrosis or apoptosis depending on mitochondrial function. Neuron. 1995;15:961–73.
80. Khodorov B, Pinelis V, Storozhevykh T, Yuravichus A, Khaspekhov L. Blockade of mitochondrial Ca^{2+} uptake by mitochondrial inhibitors amplifies the glutamate-induced calcium response in cultured cerebellar granule cells. FEBS Lett. 1999;458:162–6.
81. Nicholls DG, Budd SL, Ward MW, Castilho RF. Excitotoxicity and mitochondria. Biochem Soc Symp. 1999;66:55–67.
82. Nicholls DG, Vesce S, Kirk L, Chalmers S. Interactions between mitochondrial bioenergetics and cytoplasmic calcium in cultured cerebellar granule cells. Cell Calcium. 2003;34:407–24.
83. Kushnareva YE, Wiley SE, Ward MW, Andreyev AY, Murphy AN. Excitotoxic injury to mitochondria isolated from cultured neurons. J Biol Chem. 2005;280:28894–902.
84. Hardingham GE. Coupling of the NMDA receptor to neuroprotective and neurodestructive events. Biochem Soc Trans. 2009;37(Pt 6):1147–60.
85. Stout AK, Raphael HM, Kanterewicz BI, Klann E, Reynolds IJ. Glutamate-induced neuron death requires mitochondrial calcium uptake. Nat Neurosci. 1998;1:366–73.
86. Jekabsons MB, Nicholls DG. Bioenergetic analysis of cerebellar granule neurons undegoing apoptosis by potassium/serum deprivation. Cell Death Differ. 2006;13:1595–610.
87. Kalia LV, Kalia SK, Salter MW. NMDA receptors in clinical neurology: excitatory times ahead. Lancet Neurol. 2008;7:742–55.
88. Monti B, Contestabile A. Blockade of the NMDA receptor increases developmental apoptic elimination of granule neurons and activates caspases in the rat cerebellum. Eur J Neurosci. 2000;12:3117–23.
89. Lafon-Cazal M, Perez V, Bockaert J, Marin P. Akt mediates the anti-apoptic effect of NMDA but not that induced by potassium depolarization in cultured cerebellar granule cells. Eur J Neurosci. 2002;16:575–83.
90. Bastianelli E. Distribution of calcium-binding proteins in the cerebellum. Cerebellum. 2003;2:242–62.
91. Arai R, Winsky L, Arai M, Jacobowitz DM. Immunohistochemical localization of calretinin in the rat hindbrain. J Comp Neurol. 1991;310:21–44.
92. Rogers JH. Immunoreactivity for calretinin and other calcium-binding proteins in the cerebellum. Neuroscience. 1989;31:711–21.
93. Fortin M, Marchand R, Parent A. Calcium-binding proteins in primate cerebellum. Neurosci Res. 1998;30:155–68.
94. Faas GC, Schwaller B, Vergara JL, Mody I. Resolving the fast kinetics of cooperative binding: Ca^{2+} buffering by calretinin. PLoS Biol. 2007;5:e311.
95. Schiffmann SN, Cheron G, Lohof A, d'Alcantara P, Meyer M, Parmentier M, et al. Impaired motor coordination and Purkinje cell excitability in mice lacking calretinin. Proc Natl Acad Sci USA. 1999;96:5257–62.
96. Bearzatto B, Servais L, Rousssel C, Gall D, Baba-Aissa F, Schurmans S, et al. Targeted calretinin expression in granule cells of calretinin-null mice restores normal cerebellar functions. FASEB J. 2006;20:380–2.
97. Messer A, Plummer-Siegard J, Eisenberg B. Staggerer mutant mouse Purkinje cells do not contain detectable calmodulin mRNA. J Neurochem. 1990;55:293–302.
98. Paterlini M, Revilla V, Grant AL, Wisden W. Expression of the neuronal calcium sensor protein family in the rat brain. Neuroscience. 2000;99:205–16.
99. Burgoyne RD. Neuronal calcium sensor proteins: generating diversity in neuronal Ca^{2+} signalling. Nat Rev Neurosci. 2007;8:182–93.
100. Savidge JR, Bristow DR. Routes of NMDA- and K^+-stimulated calcium entry in rat cerebellar granule cells. Neruosci Lett. 1997;229:109–12.
101. Simpson PB, Challiss RA, Nahorski SR. Involvement of intracellular stores in the Ca^{2+} responses to N-methyl-D-aspartate and depolarization in cerebellar granule cells. J Neurochem. 1993;61:760–3.
102. Regehr WG, Atluri PP. Calcium transients in cerebellar granule cell presynaptic terminals. Biophys J. 1995;68:2156–70.
103. Dittmann JS, Regehr WG. Contributions of calcium-dependent and calcium-independent mechanisms to presynaptic inhibition at a cerebellar synapse. J Neurosci. 1996;16:1623–33.
104. Sabatini BL, Regehr WG. Control of neurotransmitter release by presynaptic waveform at the granule cell to Purkinje cell synapse. J Neurosci. 1997;17:3425–35.
105. Sabatini BL, Regehr WG. Optical measurement of presynaptic calcium currents. Biophys J. 1998;74:1549–63.
106. Beierlein M, Gee KR, Martin VV, Regehr WG. Presynaptic calcium measurements at physiological temperatures using a new class of dextran-conjugated indicators. J Neurophysiol. 2004;92:591–9.
107. Ciardo A, Meldolesi J. Regulation of intracellular calcium in cerebellar granule neurons: effect of depolarization and of glutamatergic or cholinergic stimulation. J Neurochem. 1991;56:184–91.
108. Irving AJ, Collingridge GL, Schofield JG. L-glutamate and acetylcholine mobilise Ca^{2+} from the same intracellular pool in cerebellar granule cells using transduction mechanisms with different Ca^{2+} sensitivities. Cell Calcium. 1992;13:293–301.
109. De Erausquin G, Brooken G, Costa E, Wojcik WJ. Stimulation of high affinity gamma-aminobutyric acidB receptors potentiates the depolarization-induced increase of intraneuronal ionized calcium content in cerebellar granule neurons. Mol Pharmacol. 1992;42:407–14.
110. Fohrman EB, de Erausquin G, Costa E, Wojcik WJ. Muscarinic m3 receptors and dynamics of intracellular Ca^{2+} cerebellar granule neurons. Eur J Pharmacol. 1993;245:263–71.
111. Castilho RF, Hansson O, Ward MW, Budd SL, Nicholls DG. Mitochondrial control of acute glutamate excitotoxicity in cultured cerebellar granule cells. J Neurosci. 1998;18:10277–86.
112. Ward MW, Rego AC, Frenguelli BG, Nicholls DG. Mitochondrial membrane potential and glutamate excitotoxicity in cultured cerebellar granule cells. J Neurosci. 2000;20:7208–19.

113. Rego AC, Ward MW, Nicholls DG. Mitochondria control amapa/kainate receptor-induced cytoplasmic calcium deregulation in rat cerebellar granule cells. J Neurosci. 2001;21:1893–901.
114. Jekabsons MB, Nicholls DG. In situ respiration and bioenergetic status of mitochondria in primary cerebellar granule neuronal cultures exposed continuously to glutamate. J Biol Chem. 2004;279:32989–3000.
115. Garcia-Martinez EM, Sanz-Blasco S, Karachitos A, Bandez MJ, Fernandez-Gomez FJ, Perez-Alvarez S, et al. Mitochondria and calcium flux as targets of neuroprotection caused by minocycline in cerebellar granule cells. Biochem Pharmacol. 2010;79:239–50.
116. Brenowitz SD, Regehr WG. Reliability and heterogeneity of calcium signaling at single presynaptic boutons of cerebellar granulr cels. J Neruosci. 2007;27:7888–98.
117. Zhang W, Linden DJ. Neuromodulation at single presynaptic boutons of cerebellar parallel fibers is determined by bouton size and basal action potential-evoked Ca transient amplitude. J Neurosci. 2009;29:15586–94.
118. Zhang W, Linden DJ. Calcium influx measured at single presynaptic boutons of cerebellar granule cells ascending axons and parallel fibers. Cerebellum 2010. doi:10.1007/s12311-009-0151-3.
119. Cupello A, Esposito A, Marchetti C, Pellistri F, Robello M. Calcium accumulation in neurites and cell bodies of rat cerebellar granule cells in culture: effects on $GABA_A$ receptor functions. Amino Acids. 2005;28:177–82.
120. Moulder KL, Cormier RJ, Shute AA, Zorumski CF, Mennerick S. Homeostatic effects of depolarization on Ca^{2+} influx, synaptic signaling, and survival. J Neurosci. 2003;23:1825–31.
121. Okazawa M, Abe H, Katsukawa M, Iijima K, Kiwada T, Nakanishi S. Role of calciuneurin signaling in membrane potential-regulated maturation of cerebellar granule cells. J Neurosci. 2009;29:2938–47.
122. Suzuki K, Sato M, Morishima Y, Nakanishi S. Neuronal depolarization controls brain-derived neurotrophic factor-induced upregulation of NR2C NMDA receptor via calcineurin signaling. J Neurosci. 2005;25:9535–43.
123. Popp RL, Reneau JC, Dertien JS. Cerebellar granule cells cultured from adolescent rats express functional NMDA receptors: an in vitro model for studying the developing cerebellum. J Neurochem. 2008;106:900–11.
124. Hack NJ, Sluiter AA, Balázs R. AMPA receptors in cerebellar granule cells during development in culture. Dev Brain Res. 1995;87:55–61.
125. Vallano ML, Lambolez B, Audinat E, Rossier J. Neuronal activity differentially regulates NMDA receptor subunit expression in cerebellar granule cells. J Neurosci. 1996;16:631–9.
126. Mellor JR, Merlo D, Jones A, Wisden W, Randall AD. Mouse cerebellar granule cell differentiation: electrical activity regulates the $GABA_A$ receptor α6 subunit gene. J Neurosci. 1998;18:2822–33.
127. Li L, Guerini D, Carafoli E. Calcineurin controls the transcription of Na^+/Ca^{2+} exchanger isoforms in developing cerebellar neurons. J Biol Chem. 2000;275:20903–10.
128. Maex R, De Schutter E. Synchronization of Golgi and granule cell firing in a detailed network model of the cerebellar granule cell layer. J Neurophysiol. 1998;80:2521–37.
129. Linne ML, Jalonen TO. Simulations of the cultured granule neuron excitability. Neurocomputing. 2003;52–54:583–90.
130. D'Angelo E, Nieus T, Maffei A, Armano S, Rossi P, Taglietti V, et al. Theta-frequency bursting and resonance in cerebellar granule cells: experimental evidence and modeling of a slow K^+-dependent mechanism. J Neurosci. 2001;21:759–70.
131. Roussel C, Erneux T, Schiffmann SN, Gall D. Modulation of neuronal excitability by intracellular calcium buffering: from spiking to bursting. Cell Calcium. 2006;39:455–66.
132. Nieus T, Sola E, Mapelli J, Saftenku E, Rossi P, D'Angelo E. LTP regulates burst initiation and frequency at mossy fiber−granule cell synapses of rat cerebellum: experimental observations and theoretical predictions. J Neurophysiol. 2006;95:686–99.
133. Gabbiani F, Mitgaard J, Knöpfel T. Synaptic integration in a model of cerebellar granule cells. J Neurophysiol. 1994;72:999–1009.
134. Diwakar S, Magistretti J, Goldfarb M, Naldi G, D'Angelo E. Axonal Na^+ channels ensure fast spike activation and back-propagation in cerebellar granule cells. J Neurophysiol. 2009;101:519–32.
135. McManus OB, Magleby KL. Accounting for the Ca^{2+}-dependent kinetics of single large-conductance Ca^{2+}-activated K^+ channels in rat skeletal muscle. J Physiol. 1991;443:739–77.
136. Mathie A, Clarke CE, Ranatunga KM, Veale EL. What are the roles of the many different types of potassium channel expressed in cerebellar granule cells? Cerebellum. 2003;2:11–25.
137. D'Angelo E, De Filippi G, Rossi P, Taglietti V. Ionic mechanism of electroresponsiveness in cerebellar granule cells implicates the action of a persistent sodium current. J Neurophysiol. 1998;80:493–503.
138. Brenner R, Jegla TJ, Wickenden A, Liu Y, Aldrich RW. Cloning and functional characterization of novel large conductance calcium-activated potassium channel β subunits, hkCNMB3 and hkCNMB4. J Biol Chem. 2000;275:6453–61.
139. Fakler B, Adelman JP. Control of K_{Ca} channels by calcium nano/microdomains. Neuron. 2008;59:873–81.
140. Saftenku EE. Computational study of non-homogeneous distribution of Ca^{2+} handling systems in cerebellar granule cells. J Theor Biol. 2009;257:228–44.
141. Xu T, Naraghi M, Kang H, Neher E. Kinetic studies of Ca^{2+} binding and Ca^{2+} clearance in the cytosol of adrenal chromaffin cells. Biophys J. 1997;73:532–45.
142. De Schutter E, Smolen P. Calcium dynamics in large neuronal models. In: Koch C, Segev I, editors. Methods in neuronal modeling. From ions to networks. 2nd ed. Cambridge: MIT; 1998. p. 211–50.
143. Fink CC, Slepchenko B, Moraru II, Watras J, Schaff JC, Loew LM. An image-based model of calcium waves in differentiated neuroblastoma cells. Biophys J. 2000;79:163–83.
144. Snyder SM, Palmer BM, Moore RL. A mathematical model of cardiocyte Ca^{2+} dynamics with a novel representation of sarcoplasmic reticular Ca^{2+} control. Biophys J. 2000;79:94–115.
145. Sneyd J, Tsaneva-Atanasova K, Bruce JI, Straub SV, Giovannucci DR, Yule DI. A model of calcium waves in pancreatic and parotid acinar cells. Biophys J. 2003;85:1392–405.
146. Hernjak N, Slepchenko BM, Fernald K, Fink CC, Fortin D, Moraru II, et al. Modeling and analysis of calcium signaling events leading to long-term depression in cerebellar Purkinje cells. Biophys J. 2005;89:3790–806.
147. Doi T, Kuroda S, Michikawa T, Kawato M. Inositol 1,4,5-trisphosphate-dependent Ca^{2+} threshold dynamics detect spike timing in cerebellar Purkinje cells. J Neruosci. 2005;25:950–61.
148. Patterson M, Sneyd J, Friel DD. Depolarization-induced calcium responses in sympathetic neurons: relative contributions from Ca^{2+} entry, extrusion, ER/mitochondrial Ca^{2+} uptake and release, and Ca^{2+} buffering. J Gen Physiol. 2007;129:29–56.
149. Zador A, Koch C, Brown TH. Biophysical model of a Hebbian synapse. Proc Natl Acad Sci USA. 1990;87:6718–22.
150. Saftenku EE. Estimation of the capacity of heterogeneously distributed endogenous calcium buffers in a neuron. Neurophysiology. 2009;41:111–5.
151. Schwaller B, Durussel I, Jermann D, Herrmann B, Cox JA. Comparison of the Ca^{2+}-binding properties of human recombinant calretinin-22k and calretinin. J Biol Chem. 1997;272:29663–71.

152. Weiss M, Elsner M, Kartberg F, Nilsson T. Anomalous subdiffusion is a measure for cytoplasmic crowding in living cells. Biophys J. 2004;87:3518–24.
153. Hack NJ, Wride MC, Charters KM, Kater SB, Parks TN. Developmental changes in the subcellular localization of calretinin. J Neurosci. 2000;20:RC67.
154. Hubbard MJ, McHugh NJ. Calbindin$_{28kDa}$ and calbindin$_{30kDa}$ (calretinin) are substantially localised in the particulate fraction of rat brain. FEBS Lett. 1995;374:333–7.
155. Winsky L, Kuźnicki J. Distribution of calretinin, calbindin D28k, and parvalbumin in subcellular fractions of rat cerebellum: effects of calcium. J Neurochem. 1995;65:381–8.
156. Keller DX, Franks KM, Bartol Jr TM, Sejnowski TJ. Calmodulin activation by calcium transients in the postsynaptic density of dendritic spines. PLoS ONE. 2008;3:e2045.
157. Schmidt H, Eilers J. Spine neck geometry determines spino-dendritic cross-talk in the presence of mobile endogenous calcium binding proteins. J Comput Neurosci. 2009;27:229–43.
158. Schmidt H, Kunerth S, Wilms C, Strotmann R, Eilers J. Spino-dendritic cross-talk in rodent Purkinje neurons mediated by endogenous Ca^{2+}-binding proteins. J Physiol. 2007;581(Pt 2):619–29.
159. Schaad NC, De Castro E, Nef S, Hegi S, Hinrichsen R, Martone ME, et al. Direct modulation of calmodulin targets by the neuronal calcium sensor NCS-1. Proc Nat Acad Sci USA. 1996;93:9253–8.
160. Spilker C, Richter K, Smalla KH, Manahan-Vaughan D, Gundelfinger ED, Braunewell KH. The neuronal EF-hand calcium-binding protein visinin-like protein-3 is expressed in cerebellar Purkinje cells and shows a calcium-dependent membrane association. Neuroscience. 2000;96:121–9.
161. Jheng FF, Wang L, Lee L, Chang LS. Functional contribution of Ca^{2+} and Mg^{2+} to the intermolecular interaction of visinin-like proteins. Protein J. 2006;25:250–6.
162. Jeromin A, Muralidhar D, Parameswaran MN, Roder J, Fairwell T, Scarlata S, et al. N-terminal myristolation regulates calcium-induced conformational changes in neuronal calcium sensor-1. J Biol Chem. 2004;279:27158–67.
163. van Kan PL, Gibson AR, Houk JC. Movement-related inputs to intermediate cerebellum of the monkey. J Neurophysiol. 1993;69:74–94.
164. D'Errico A, Prestori F, D'Angelo E. Differential induction of bidirectional long-term changes in neurotransmitter release by frequency-coded patterns at the cerebellar input. J Physiol. 2009;587(Pt 24):5843–57.
165. Cathala L, Misra C, Cull-Candy S. Developmental profile of the changing properties of NMDA receptors at cerebellar mossy fiber−granule cell synapses. J Neurosci. 2000;20:5899–905.
166. Colegrove SL, Albrecht MA, Friel DD. Quantitative analysis of mitochondrial Ca^{2+} uptake and release pathways in sympathetic neurons. Reconstruction of the recovery after depolarization-evoked $[Ca^{2+}]_i$ elevations. J Gen Physiol. 2000;115:371–88.
167. Young KW, Bampton ET, Pinòn L, Bano D, Nicotera P. Mitochondrial Ca^{2+} signalling in hippocampal neurons. Cell Calcium. 2008;43:296–306.
168. Blum R, Petersen OH, Verkhratsky A. Ca^{2+} imaging of intracellular organelles: endoplasmic reticulum. In: Verkhratsky A, Petersen OH, editors. Calcium measurement methods: Neuromethods, vol. 43. New York: Humana; 2010. p. 147–67.
169. Albrecht MA, Colegrove SL, Hongpaisan J, Pivovarova NB, Andrews SB, Friel DD. Multiple modes of calcium-induced calcium release in sympathetic neurons I: attenuation of endoplasmic reticulum Ca^{2+} accumulation at low $[Ca^{2+}]_i$ during weak stimulation. J Gen Physiol. 2001;118:83–110.
170. Choi YM, Kim SH, Chung S, Uhm DY, Park MK. Regional interaction of endoplasmic reticulum Ca^{2+} signals between soma and dendrites through rapid luminal Ca^{2+} diffusion. J Neurosci. 2006;26:12127–36.
171. Migliore M, Shepherd GM. Emerging rules for the distributions of active dendritic conductances. Nat Rev Neurosci. 2002;3:362–70.
172. Veiko VP, Golubok AO, Zuong Z, Varkentina NV, Yakovlev EB. Combined nanoprobes for scanning microscopy: laser technology for processing and testing. Proc SPIE. 2008;6879:68791W.1–68791W.10.
173. Sabatini B, Svoboda K. Analysis of calcium channels in single spines using optical fluctuation analysis. Nature. 2000;408:589–93.
174. Westenbroek RE, Sakurai T, Elliott EM, Hell JW, Starr TV, Snutch TP, et al. Immunochemical identification and subcellular distribution of the alpha 1A subunits of brain calcium channels. J Neurosci. 1995;15:6403–18.
175. Leitch B, Szostek A, Lin R, Shevsova O. Subcellular distribution of L-type calcium channel subtypes in rat hippocampal neurons. Neuroscience. 2009;164:641–57.
176. Hackney CM, Mahendrasingam S, Penn A, Fettiplace R. The concentrations of calcium buffering proteins in mammalian cohlear hair cells. J Neurosci. 2005;25:7867–75.
177. Schmidt H, Schwaller B, Eilers J. Calbindin D28k targets myo-inositol monophosphatase in spines and dendrites of cerebellar Purkinje neurons. Proc Natl Acad Sci USA. 2005;102:5850–5.
178. Lörincz A, Rozsa B, Katona G, Vizi ES, Tamas G. Differential distribution of NCX1 contributes to spine-dendrite compartmentalization in CA1 pyramidal neurons. Proc Natl Acad Sci USA. 2007;104:1033–8.
179. Maravall M, Mainen ZF, Sabatini BL, Svoboda K. Estimating intracellular calcium concentrations and buffering without wavelength ratioing. Biophys J. 2000;78:2655–67.
180. Sabatini BL, Oertner TG, Svoboda K. The life cycle of Ca^{2+} ions in dendritic spines. Neuron. 2002;33:439–52.
181. Fierro L, DiPolo R, Llano I. Intracellular calcium clearance in Purkinje cell somata from rat cerebellar slices. J Physiol. 1998;510(Pt 2):499–512.
182. Landolfi B, Curci S, Debellis L, Pozzan T, Hofer AM. Ca^{2+} homeostasis in the agonist-sensitive internal store: functional interactions between mitochondria and the ER measured in situ in intact cells. J Cell Biol. 1998;142:1235–43.
183. Czyz A, Kiedrowski L. Inhibition of plasmalemmal Na+/Ca2+ exchange by mitochondrial Na+/Ca2+ exchange inhibitor 7-chloro-5-(2-chlorophenyl)-1, 5-dihydro-4, 1-benzothiazepin-2 (3 H)-one (CGP-37157) in cerebellar granule cells. Biochem Pharmacol. 2003;66:2409–11.
184. Billups B, Forsythe ID. Presynaptic mitochondrial calcium sequestration influences transmission at mammalian central synapses. J Neurosci. 2002;22:5840–7.
185. Vay L, Hernandez-SanMiguel E, Lobatón CD, Moreno A, Montero M, Alvarez J. Mitochondrial free $[Ca^{2+}]$ levels and the permeability transition. Cell Calcium. 2009;45:243–50.
186. Contreras L, Drago I, Zampese E, Pozzan T. Mitochondria: the calcium connection. Biochim Biophys Acta. 2010;1797:607–18.
187. Higgins ER, Goel P, Puglisi JL, Bers DM, Cannell M, Sneyd J. Modelling calcium microdomains using homogenisation. J Theor Biol. 2007;247:623–44.
188. Albrecht MA, Colegrove SL, Friel DD. Differential regulation of ER Ca^{2+} uptake and release rates accounts for multiple modes of Ca^{2+}-induced Ca^{2+} release. J Gen Physiol. 2002;119:211–33.
189. Pozzan T, Rudolf R. Measurements of mitochondrial calcium in vivo. Biochym Biophys Acta. 2009;1787:1317–23.